Prognostic prediction signature and molecular subtype for liver cancer: A CTC/CTM-related gene prediction model and independent external validation

LING XU[1], QIANSHENG WU[1], KAI ZHAO[2], XIANGYU LI[3] and WEI YAO[4]

[1]Department of Nursing, Tongji Hospital Affiliated to Tongji Medical College, Huazhong University of Science and Technology, Wuhan, Hubei 430030, P.R. China; [2]Department of Biliary and Pancreatic Surgery/Cancer Research Center Affiliated Tongji Hospital, Tongji Medical College, Huazhong University of Science and Technology, Wuhan, Hubei 430030, P.R. China; [3]Department of Thoracic Surgery, Tongji Hospital Affiliated with Tongji Medical College, Huazhong University of Science and Technology, Wuhan, Hubei 430030, P.R. China; [4]Department of Oncology, Tongji Hospital Affiliated with Tongji Medical College, Huazhong University of Science and Technology, Wuhan, Hubei 430030, P.R. China

Received March 26, 2024; Accepted July 31, 2024

DOI: 10.3892/ol.2024.14664

Abstract. Liver cancer is the second leading cause of tumor-related death worldwide, and a serious threat to lives and health. Circulating tumor cells (CTCs) facilitate the progression of various cancers, including liver cancer. The relationship between CTC/circulating tumor microemboli-related genes (CRGs) and the prognosis of liver cancer is unclear. The aim of the present study was to identify CTC/circulating tumour microemboli-related genes (CRGs) in hepatocellular carcinoma and to investigate their clinical significance. Transcriptomic data from The Cancer Genome Atlas (International Cancer Genome Consortium (ICGC) and GSE117623 databases were combined, and differentially expressed CRGs were identified. These were subsequently analyzed via least absolute shrinkage and selection operator and multivariate Cox analyses, and a five-gene risk signature was constructed. The signature was validated in the ICGC and GSE14520 dataset with survival analysis and receiver operating characteristic curve analysis. Immunocyte infiltration, tumor mutation burden (TMB), tumor immune dysfunction and exclusion (TIDE), and the somatic mutation rate were also compared between high- and low-risk groups, based on the median predictive index, to further evaluate the immunotherapeutic value of the model. Molecular subtypes of liver cancer were characterized by the non-negative matrix factorization method and potential therapeutic compounds were evaluated for different subtypes. Nomograms were utilized to predict the prognosis of patients, and the signature was compared with previous literature models. Additionally, the biological function of one of the CRGs, tumor protein p53 inducible protein 3 (TP53I3), in liver cancer was further explored through *in vitro* experiments. Analysis of the prognostic characteristics of the five CRGs led to the identification of two liver cancer subtypes. Patients in the low-risk group had a longer survival compared with those in the high-risk group, and patients in the latter group were associated with a higher TMB, immunocyte infiltration and somatic mutation rate, and lower TIDE scores. The prognostic profile was validated in the ICGC and GSE14520 datasets and exhibited a good predictive performance. *In vitro* analysis showed that the knockdown of TP53I3 suppressed liver cancer cell proliferation. In summary, CRGs were used to develop a new prognostic signature to predict the prognosis of patients with liver cancer. This signature may be used to assess the prognosis of patients and may provide new insights for clinical management strategies. In addition, TP53I3 is potentially a therapeutic target for liver cancer.

Correspondence to: Professor Wei Yao, Department of Oncology, Tongji Hospital Affiliated with Tongji Medical College, Huazhong University of Science and Technology, 1095 Liberation Avenue, Wuhan, Hubei 430030, P.R. China
E-mail: yw13557@163.com

Professor Xiangyu Li, Department of Thoracic Surgery, Tongji Hospital Affiliated with Tongji Medical College, Huazhong University of Science and Technology, 1095 Liberation Avenue, Wuhan, Hubei 430030, P.R. China
E-mail: lixy523wh@163.com

Abbreviations: CTC, circulating tumor cells; CTMs, circulating tumor microemboli; CRGs, CTCs/CTM-related genes; DEGs, differentially expressed genes; GO, Gene Ontology; GSEA, gene set enrichment analysis; GSVA, gene set variation analysis; ICGC, International Cancer Genome Consortium; KEGG, Kyoto Encyclopedia of Genes and Genomes; LASSO, least absolute shrinkage and selection operator; NMF, non-negative matrix factorization; PPI, protein-protein interaction; ROC, receiver operating characteristic; TCGA, The Cancer Genome Atlas; TMB, tumor mutation burden; TIDE, tumor immune dysfunction and exclusion

Key words: circulating tumor cells, liver cancer, prognostic signature, immune microenvironment, immune infiltration

Introduction

Primary liver cancer is among the six most widespread malignancies worldwide, and has the third highest mortality rate globally (1-3). Liver cancer is closely associated with chronic liver disease in >90% of cases, and causes of cirrhosis are important risk factors for liver cancer. Alcohol consumption, diabetes, obesity-induced non-alcoholic steatohepatitis and hepatitis B and V viruses are all critical risk elements for liver cancer, in addition to biliary cirrhosis and hemochromatosis (4,5). Currently, the primary treatment options for liver cancer are radical resection or liver transplantation. However, for patients with advanced, recurrent liver cancer or those who are not suitable for surgery, the prognosis remains unsatisfactory. Despite some advances in the diagnosis, treatment and management of liver cancer, its overall survival remains poor due to the high rates of relapse, vascular invasion or distant metastasis (6). Therefore, it is urgently necessary to explore effective and representative biomarkers and new predictive tools.

Circulating tumor cells (CTCs) are tumor cells that have been shed from a primary or metastatic lesion into the bloodstream, which are rare in healthy individuals (7-9). CTCs exist as single cells or multicellular aggregates known as circulating tumour microemboli (CTMs) (10). Studies in mouse models have confirmed that CTMs are more metastatic than individual CTCs, with results suggesting that the injection of clusters of aggregated cancer cells significantly increases the formation of tumours compared to the injection of the same number of individual cancer cells into mice (11-13). Heterotopic CTMs contain many helper cells, such as red blood cells, fibroblasts and immune cells, which contribute to the metastatic survival of CTMs, rather than just an aggregation of individual cancer cells (14). As an essential component of liquid biopsy technology, CTCs play an essential role in the diagnosis and treatment of cancer, carrying heterogeneous information about the primary tumor and serving as an effective biomarker and modeling tool. Researchers have found that CTCs serve a key role in the metastatic process of tumors. Therefore, the isolation and identification of CTCs with non-invasive biopsy can be widely applied for the early diagnosis, real-time efficacy monitoring and prognosis evaluation of tumors (12,15-18). In general, it has been shown that higher levels of CTCs are associated with a worse outcome in patients with tumors. For example, in two studies of patients with liver cancer, the duration of survival was significantly shorter and associated with poor clinical features in the CTC-positive cohort (19,20). Similarly, Sun *et al* (21) found that the risk of tumor recurrence increased in patients with liver cancer when the preoperative CTC count was ≥2/7.5 ml, particularly at a-fetoprotein levels of ≤400 ng/ml. With advances in technology, and the genomic, transcriptomic and proteomic analysis of CTCs at the single-cell level, as well as the refinement of CTC *in vitro* models, our understanding of the critical role of CTCs in cancer has been improved (22,23). Nevertheless, the biological functions of CTCs in tumors at the molecular level have not been fully elucidated. Therefore, the present study aimed to identify the CTC/CTM-related genes (CRGs) in liver cancer and explore their clinical significance.

In the present study, a comprehensive analysis of the transcriptomic data and clinical information of liver cancer in The Cancer Genome Atlas (TCGA) and the International Cancer Genome Consortium (ICGC) databases was performed. Analysis of these data in combination with mRNA data associated with liver cancer from the GSE117623 dataset led to the identification of 258 CRGs. Subsequently, a prognostic model and risk subgroups for patients with liver cancer were constructed based on five CRGs, and the associations between different subgroups of patients and immune markers such as immune infiltration, immune checkpoints and tumor mutation burden (TMB) were analyzed. Finally, the detection efficacy and clinical value of the model were evaluated, and chemotherapeutic agents with potential therapeutic value were screened.

Materials and methods

Data sources. The transcriptome profiles and the corresponding clinicopathological data of patients with liver cancer were obtained from TCGA database (https://portal.gdc.cancer.gov/) as the training cohort. In addition, RNA-sequencing (RNA-seq) data and clinical trait information from patients with liver cancer were downloaded from the ICGC database (LIRI-JP dataset; https://icgc.org/) and Gene Expression Omnibus (GEO; http://www.ncbi.nlm.nih.gov/) for validation. Specifically, 12,518 CRGs in the GSE117623 dataset were downloaded from the GEO database (24). Transcriptomic and matched clinical data from the IMvigor210 cohort of patients treated with anti-PD-L1 were collected (research-pub.gene.com/IMvigor210CoreBiologies) to explore the value of model genes in assessing response to immunotherapy (25).

Identification of candidate genes. To acquire the differentially expressed genes (DEGs) associated with CTCs/CTMs, the limma R package (version 2.7, bioinf.wehi.edu.au/limma) was used to process the RNA-seq data using a false discovery rate (FDR) <0.05 and |log2 (fold change)|>2 as the cutoff criteria. A Venn diagram was then constructed using a Venn webtool (http://bioinformatics.psb.ugent.be/webtools/Venn/) to illustrate the intersection among TCGA-DEGs, ICGC-DEGs and genes from the GSE117623 dataset. These intersected genes were considered to be the CRGs.

Pathway enrichment and protein-protein interaction (PPI) network analysis. Gene Ontology (GO) and Kyoto Encyclopedia of Genes and Genomes (KEGG) enrichment analyses were conducted to explore the functional roles and pathways associated with the CRGs using the clusterProfiler R package (version 3.19) (26). The cut-offs were set as P<0.05 and FDR <0.05. Gene set enrichment analysis (GSEA) was performed to investigate the common biological pathways (27) using cp.kegg.v7.1.symbols.gmt as a reference gene set with a threshold of P<0.05, to screen for key enriched pathways in different risk groups. In addition, interactions among the CRGs were illustrated by the construction of a PPI network using the STRING database (https://string-db.org/), with an interaction score >0.7 being considered significant. Moreover, Cytoscape software was utilized to visually represent the PPI network. Specifically, the Cytoscape plug-in Molecular Complex Detection (MCODE) (version 2.0.3) was utilized to

identify the highly interconnected modules of the PPI network with the following criteria: Degree cut-off, 2; node score cut-off, 0.2; k-core, 2; and max. depth, 100 (28). In addition, another Cytoscape plug-in, cytoHubba (version 0.1), was used to rank the nodes in the network according to their network functionality (29). The gene set variation analysis (GSVA) package (version 3.19) was used to explore the signaling pathways between high- and low-risk groups (30).

Construction and validation of the risk prognostic model. Univariate Cox regression analysis was performed to determine the prognostic CRGs and the CRGs associated with survival time, with $P<0.01$ considered to be statistically significant. Then, least absolute shrinkage and selection operator (LASSO) penalized Cox regression analysis was performed to further filter prognostic CRGs associated with the overall survival (OS) of patients with liver cancer (31). Subsequently, a risk signature was developed via stepwise multivariate Cox proportional hazards regression analysis. Prognostic gene signatures were constructed based on linear combinations of regression coefficients derived by multiplying the LASSO Cox regression model coefficients by their mRNA expression levels (32): Risk score=$\sum$ (βmRNA x mRNA)n, where β represents the regression coefficient for the mRNA, mRNA represents the expression level of the mRNA, and n represents the specific gene. Receiver operating characteristic (ROC) curves and Kaplan-Meier curves were constructed to evaluate the predictive performance of the prognostic model in TCGA cohort. pheatmap R package (version 1.0.12; cran.r-project.org/web/packages/pheatmap/index.html) to plot images describing gene expression heatmaps, risk scores and OS for high and low risk groups. Data from the ICGC and GEO databases were used as external validation data to test the predictive capability of the model.

Identification of liver cancer subtypes. A non-negative matrix factorization (NMF) clustering algorithm was utilized to analyze the five signature genes in the risk score model, and determine the subtypes of CRGs in liver cancer using the NMF R package (version 0.27) (33). Using conformal, scatter and silhouette features, the optimal number of clusters with n=2 was determined.

Establishing the predictive nomogram. Nomograms are widely used as a tools for the prognostic analysis of patients with tumors (34). A simplified liver cancer nomogram was constructed for each dataset based on the CRG model and its predictive performance was evaluated by plotting calibration curves.

Bioinformatics analysis of the prognostic signature. The association between the low- and high-risk groups and clinical characteristics were explored using Chi-square tests, and the results were displayed as a heatmap. In addition, the associations between the signature genes and immune cell infiltration were analyzed. Six algorithms, namely CIBERSORT-ABS (35), TIMER (36) (https://cistrome.shinyapps.io/timer/), QUANTISEQ (37), MCPCOUNTER (38), XCELL (39) and EPIC (40,41), were used to evaluate the differences in the immune microenvironment between the two risk groups. Tumor-associated immune comprehensive score was assessed via ImmunoPhenoScore in R package IOBR (42) (version 0.99.9, https://github.com/IOBR/IOBR). Waterfall plots for the two risk groups were produced using the maftools (github.com/PoisonAlien/maftools) R package (version 3.19). Differences in the expression of major histocompatibility complex (MHC) molecules, human leukocyte antigen (HLA) signature, chemokines and potential immune checkpoints were also compared between the two groups. To investigate the association between signature genes and immune subtypes, 'Subtypes' module of the TISIDB database (http://cis.hku.hk/TISIDB/index.php). Pearson correlation coefficients of the signature genes expression with the immune checkpoints (PD-1, PD-L1 and CTLA4) were calculated using R language to assess the correlation. In this study, the OCLR algorithm and the Primary Cell Biology Consortium (PCBC, https://progenitorcells.org/) stemness score model were used to calculate the mRNAsi of cells in the TCGA-LIHC dataset and to assess the correlation between the stemness index and the risk score (43). Pearson correlation coefficients of the signature genes expression with the immune checkpoints were calculated using the R language to assess the correlation.

Screening potential therapeutic small molecule drugs for liver cancer. To identify small molecule compounds that may be suitable for the treatment of liver cancer, the pRRophetic (genemed.uchicago.edu/~pgeeleher/pRRophetic/) R package (version 3.19) was used to calculate the half-maximal inhibitory concentration (IC_{50}) based on data from the Genomics of Drug Sensitivity in Cancer database (44).

Cell culture and transfection. HepG2 and MHCC97H human liver cancer cells (cat. nos. CTCC-001-0014 and CTCC-400-0192, respectively) were obtained from the Meisen Chinese Tissue Culture Collections. The cell lines were authenticated by short tandem repeat testing. Both cell lines were cultivated in high-glucose Dulbecco's modified Eagle's medium (Gibco; Thermo Fisher Scientific, Inc.) supplemented with 10% fetal bovine serum (Gibco; Thermo Fisher Scientific, Inc.) at 37˚C in 5% CO_2. Two small interfering RNA (siRNAs) targeting tumor protein p53 inducible protein 3 (TP53I3), namely si-TP53I3-1 and si-TP53I3-2, and an siRNA negative control were synthesized by and purchased from Sangon Biotech Co., Ltd. The sequences of siRNAs are listed in Table SI. Cell transfection was conducted in 6-well plates when cell confluence was 60-70%, with a final siRNA concentration of 50 nM per well. Transfection of the liver cancer cells was performed using Lipofectamine® 2000 reagent (Invitrogen; Thermo Fisher Scientific, Inc.) following the manufacturer's instructions. Transfection was performed for 6-8 h at 37˚C in 5% CO_2. The cells were harvested at 24 h post-transfection for reverse transcription-quantitative PCR (RT-qPCR) analysis and at 48 h post-transfection for western blot and *in vitro* functional assessment.

Western blot analysis. Cells were lysed on ice with RIPA buffer (Wuhan Boster Biological Technology, Ltd.) containing protease inhibitor cocktail (MedChemExpress) for 20 min. The protein contents of the cell lysates were quantified using a BCA protein assay kit (Beyotime Institute of Biotechnology). Then, 30 μg protein/lane was separated by 10% SDS-PAGE

(Boster Biological Technology) and transferred to PVDF membranes (EMD Millipore). The membranes were blocked with 5% defatted milk at room temperature for 2 h, then incubated with anti-TP53I3 (#14828-1-AP; 1:1,000; Proteintech Group, Inc.) and anti-ACTB (#AC006; 1:3,000; ABclonal Biotech Co., Ltd.). primary antibodies at 4˚C for 12-16 h, followed by HRP-conjugated Affinipure goat anti-rabbit IgG (H+L) (SA00001-2; 1:5,000; Proteintech) secondary antibodies at room temperature for 2 h, and the signal was detected using Pierce® ECL Western Blotting Substrate (Thermo Fisher Scientific, Inc.). Finally, the bands were detected and analyzed using ChemiDoc™ XRS+ with Image Lab™ software (version 6.0, Bio-Rad Laboratories, Inc.).

RT-qPCR. Total RNA was extracted from cells using FreeZol reagent (Vazyme Biotech Co., Ltd.) and synthesized into cDNA using PrimeScript™ RT Master Mix (Takara Bio, Inc.), according to the manufacturer's instructions. qPCR was then carried out using the CFX96 Real-Time PCR System (Bio-Rad Laboratories, Inc.) with the SYBR Green PCR kit (Thermo Fisher Scientific, Inc.) according to the standard protocol. The thermocycling conditions used were as follows: 95˚C for 30 sec pre-cycling, and then 40 cycles of 95˚C for 10 sec and 60˚C for 30 sec. The primer pairs were synthesized by Sangon Biotech Co., Ltd. and their sequences are presented in Table SII. The relative expression of TP53I3 was calculated using the formula $2^{-\Delta\Delta Cq}$ with GAPDH as the reference gene (34).

Cell proliferation assay. Cell Counting Kit 8 (CCK-8) assay (ABclonal Biotech Co., Ltd.) was utilized to assess the proliferation ability of the cells. Cells (3,000/well) were plated in a 96-well plate and incubated overnight at 37˚C to allow adhesion. At 24, 48 and 74 h, 100 μl 10% CCK-8 solution was added to each well and the cells were cultured in a cell incubator for 2 h, after which absorbance was measured at 450 nm using a microplate reader (Thermo Fisher Scientific, Inc.).

Colony formation assay. Cells were seeded into 6-well plates at a concentration of 1,000 cells/well. The cells were cultured at 37˚C with 5% CO_2 in fresh medium and allowed to grow for 14 days. The colonies were then fixed for 15 min at room temperature in 4% paraformaldehyde (Wuhan Servicebio Technology Co., Ltd.), and stained with crystal violet (0.5% wt./vol.) at room temperature for 15 min. Finally photographs of the plates were taken and the colonies were quantified using an inverted microscope (Guangzhou Micro-shot Technology Co., Ltd.). The number of colonies was counted manually. Each independently counted colony refers to a cell cluster of ≥50 cells. The experiment was repeated three times.

5-Ethynyl-2'-deoxyuridine (EdU) detection. The BeyoClick™ EdU-555 Cell Proliferation Kit (Beyotime Institute of Biotechnology) was employed to investigate the proliferation rate of the human liver cancer cells according to the manufacturer's protocols. Briefly, after incubation with 1X EdU (10 μM) solution for 2 h at 37˚C, cells were fixed with paraformaldehyde (4%) for 30 min at room temperature, then permeabilized with 0.3% Triton X-100 for 15 min and finally stained with Hoechst 33342 and 4',6-diamidino-2-phenylindole in the absence of light for 30 min at room temperature. Finally, the cells were imaged by fluorescence microscopy.

Statistical analysis. Bioinformatics analysis and mapping were accomplished using R software. Survival rates were compared using Kaplan-Meier analysis with the calculation of P-values using log-rank tests, or the 2-stage test in the plot with late-stage crossover (cran.r-project.org/web/packages/TSHRC/TSHRC.pdf). In addition, the Chi-square test was used for comparisons between categorical variables, and unpaired Student's t-test was utilized to evaluate the discrepancies between the two risk groups. Correlations between variables were assessed using Spearman's correlation test. The cell groups were compared by one-way ANOVA followed by Dunnett's post hoc tests. For each statistical analysis, $P<0.05$ was considered to indicate a statistically significant result.

Results

Differentially expressed CRGs. The liver cancer (liver hepatocellular carcinoma) gene expression profiles were downloaded from TCGA and ICGC portals and 1,622 and 628 DEGs, respectively, were screened out using the limma R package. The DEGs from TCGA and ICGC databases are shown as volcano plots in Fig. 1A and B, respectively. A Venn diagram was then constructed to filter out the differentially expressed CRGs (Fig. 1C). The intersection of the DEGs from TCGA and ICGC databases with the 12,518 CRGs from GSE117623 yielded a total of 258 differentially expressed CRGs (Table SIII).

PPI network construction. To investigate the interrelationship of the differentially expressed CRGs and identify hub genes, a PPI network was constructed and module analysis performed to determine co-expression networks. Firstly, the 258 differentially expressed CRGs were uploaded to the STRING database, and the minimum required interaction score was set to 0.7, which indicates a strong interaction between the CRGs. The STRING interactions were then analyzed using Cytoscape and the resulting co-expression network, which contained 155 nodes and 2,731 edges, is shown in Fig. 2A. In addition, modules with >50 genes were identified using the MCODE plug-in and 10 hub genes in that module, namely topoisomerase IIa, cyclin B2, cell division cycle associated 8 (CDCA8), BIRC5, aurora kinase B, cyclin B1, BUB1 mitotic checkpoint serine/threonine kinase (BUB1), BUB1B, kinesin family member 20A and TTK protein kinase, were characterized using the cytoHubba plug-in (Fig. 2B). This included 57 nodes and 1,497 edges. These potential hub genes may be instrumental in the biological progression of liver cancer.

GO and KEGG enrichment analyses. To explore the biological categories and biological processes associated with the differentially expressed CRGs, GO and KEGG enrichment analyses were conducted using R software, and the enrichment results are shown in bubble charts (Fig. 2C and D). The GO enrichment analysis revealed that the differentially expressed CRGs were principally concentrated in the biological process terms ‘nuclear division’, ‘organelle fission’, ‘chromosome segregation’ and ‘mitotic nuclear division’. In addition, the main

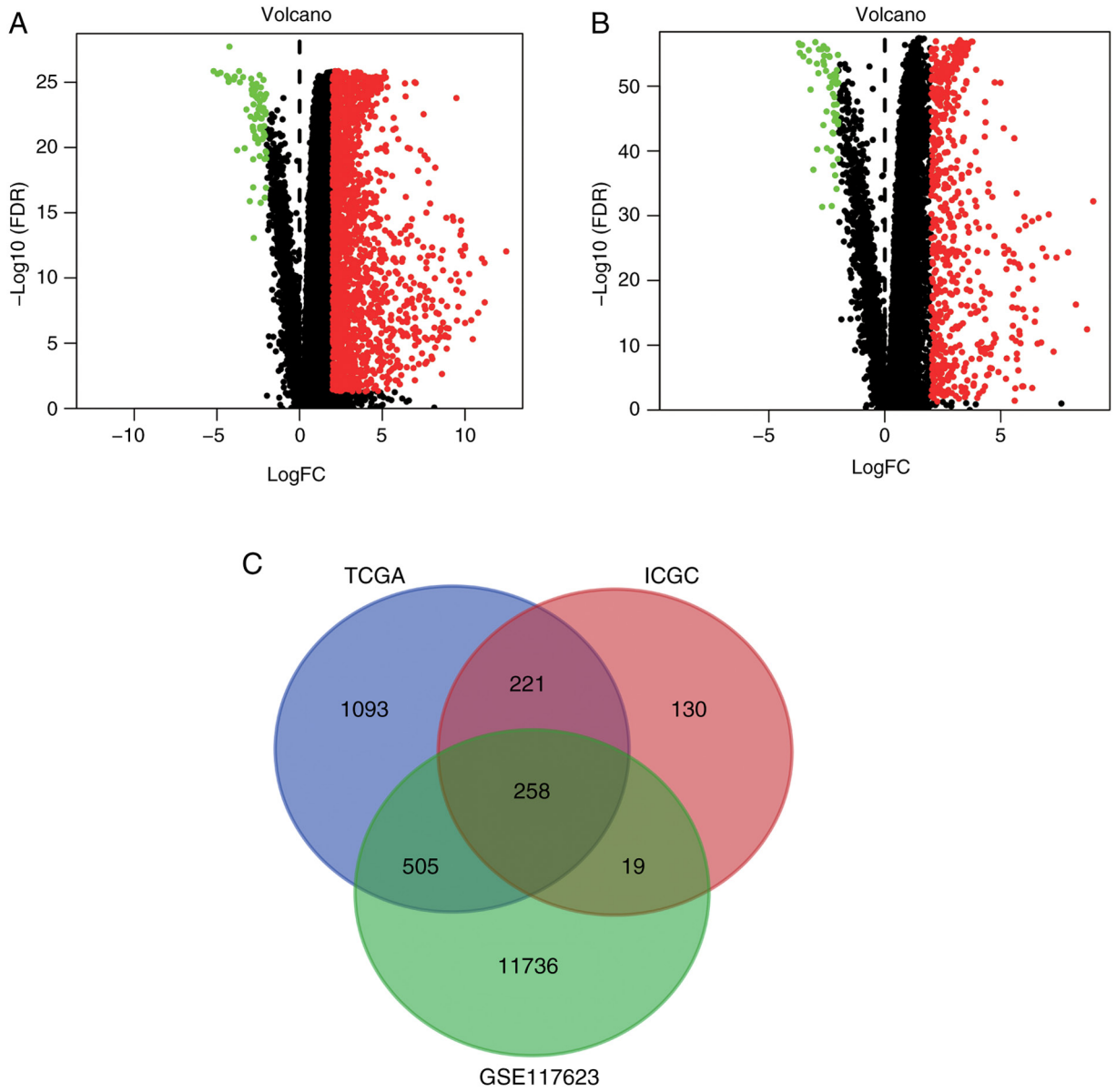

Figure 1. Identification of CRGs. Volcano plots of the differentially expressed genes in (A) TCGA and (B) ICGC datasets. (C) Venn diagram showing the intersection of the TCGA, ICGC and GSE117623 datasets, from which a total of 258 CRGs were identified. CRGs, circulating tumor cell/circulating tumor microemboli-related genes; TCGA, The Cancer Genome Atlas; ICGC, International Cancer Genome Consortium; FDR, false discovery rate; FC, fold change.

cellular component terms included 'chromosomal region', 'chromosome, centromeric region', 'spindle' and 'kinetochore'. Moreover, the molecular function terms associated with the CRGs were 'tubulin binding', 'microtubule-binding', 'ATPase activity' and 'motor activity' (Fig. 2C). Regarding the KEGG analysis, the primary terms are shown in Fig. 2D, which reveals that the differentially expressed CRGs were particularly enriched in 'cell cycle', 'microRNAs in cancer', 'p53 signaling pathway' and 'cellular senescence'.

Construction of a prognostic model and validation of the model in the ICGC cohort. Univariate Cox regression analysis demonstrated that 88 CRGs were strongly associated with survival in patients with liver cancer (P<0.01), all of which were prognostic risk factors (Fig. 3A). Then, the 88 CRGs were regression penalized using LASSO Cox regression to exclude relatively insignificant parameters (Fig. 3B and C). Stepwise multivariate Cox regression was subsequently employed to construct a predictive signature for patients with liver cancer in TCGA cohort (Fig. 3D). The five genes in the signature were CDCA8, TP53I3, hepatitis A virus cellular receptor 1 (HAVCR1), MYCN proto-oncogene (MYCN) and thioredoxin reductase 1 (TXNRD1). The formula for risk score calculation was as follows: Risk score=(0.0826 x expression level of CDCA8) + (0.0112 x expression level of TP53I3) + (0.0824 x expression level of MYCN) + (0.0376 x expression level of HAVCR1) + (0.0120 x expression level of TXNRD1) (Table SIV). Patients in TCGA cohort were classified into high- and low-risk groups using the median predictive index as the cut-off point. As Fig. 4A shows, the low-risk group was significantly associated with improved survival (P<0.05). To evaluate the predictive ability of this prognostic signature, an ROC analysis of the risk score was conducted. The area under the curve (AUC) values predicted from the ROC curves for 1-, 3- and 5-year OS were

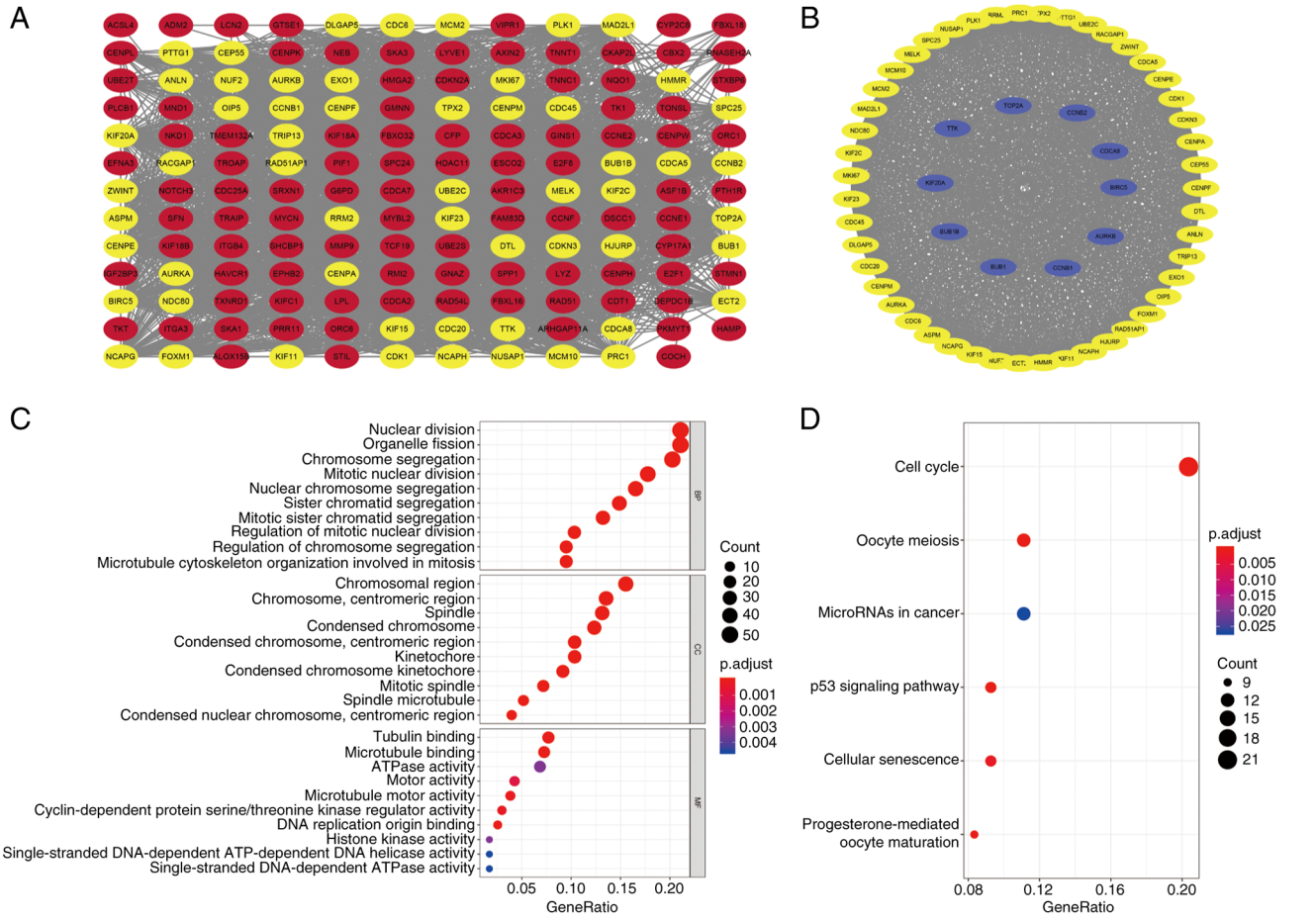

Figure 2. Protein-protein interaction networks and functional annotation of the CRGs. (A) Interaction network comprising 155 genes, with an interaction score >0.7 set as significant. Yellow represents module 1, with >50 genes by the Molecular Complex Detection algorithm. (B) In module 1, blue represents the top 10 hub genes calculated by cytoHubba. Functional annotation of these differentially expressed CRGs based on (C) Gene Ontology enrichment analysis and (D) Kyoto Encyclopedia of Genes and Genomes analysis. CRGs, circulating tumor cell/circulating tumor microemboli-related genes; p.adjust, adjusted P-value.

0.804, 0.736 and 0.707, respectively (Fig. 4B). In Fig. 4C, the upper panel shows the expression heat map of the five prognostic model genes in the high- and low subgroups, the middle panel reveals that the risk of patients with liver cancer increases as risk score increases, and the lower panel demonstrates the poor OS of the patients in the high-risk group compared with those in the low-risk group. To validate the predictive power of the signature, the same formula was used to analyze the risk score of each patient in the ICGC dataset, for independent external validation. The Kaplan-Meier curves also displayed a poor prognosis of patients in the high-risk group in this dataset (P<0.05; Fig. 4D). In addition, the ROC curve showed the strong predictive ability of the risk-score signature for prognosis, with AUCs for the prediction of 1-, 3- and 5-year OS of 0.714, 0.730 and 0.726, respectively (Fig. 4E). Also, the expression of the five CRGs and the mortality of the patients increased as the risk scores increased (Fig. 4F).

Independent prognostic role of the gene signature. To investigate whether the CTC/CTM-associated 5-gene signature could be an independent prognostic factor for patients with liver cancer, the prognostic value of this signature was compared with that of several clinicopathological factors, including age, sex, grade and American Joint Committee on Cancer (AJCC) stage in both cohorts using univariate and multivariate Cox regression analyses. For TCGA cohort, 365 valid patients were included, 182 in the high-risk group and 183 in the low-risk group. Univariate Cox analysis indicated that risk score [P<0.001; hazard ratio (HR), 1.258; 95% confidence interval (95% CI), 1.183-1.338)], AJCC stage (P<0.001; HR, 1.658; 95% CI, 1.340-2.053) and T status (P<0.001; HR, 1.633; 95% CI, 1.332-2.003) were candidate factors. Further multivariate Cox regression analysis emphasized that risk score was an independent risk factor for patients with liver cancer (P<0.001; HR, 1.227; 95%CI, 1.142-1.318) (Fig. 4G). For the ICGC cohort, 229 patients were included, 59 in the high-risk group and 170 in the low-risk group. Univariate Cox regression analysis demonstrated that sex (P=0.033; HR, 0.505; 95% CI, 0.270-0.946), risk score (P=0.010; HR, 1.076; 95% CI, 1.017-1.137) and tumor stage (P<0.001; HR, 2.252; 95% CI, 1.543-3.287) were potential risk factors. Multivariate Cox regression analysis also indicated that sex (P=0.004; HR, 0.389; 95% CI, 0.204-0.740), risk score (P=0.030; HR, 1.070; 95% CI, 1.006-1.138 and tumor stage (P<0.001; HR, 2.330; 95% CI, 1.601-3.391) were independent predictors for patients in the ICGC cohort (Fig. 4H). In conclusion, these findings indicated that the 5-CRG risk signature was closely associated with the clinical characteristics of patients with liver cancer, had a fine predictive capacity and has potential as a prognostic indicator for these patients.

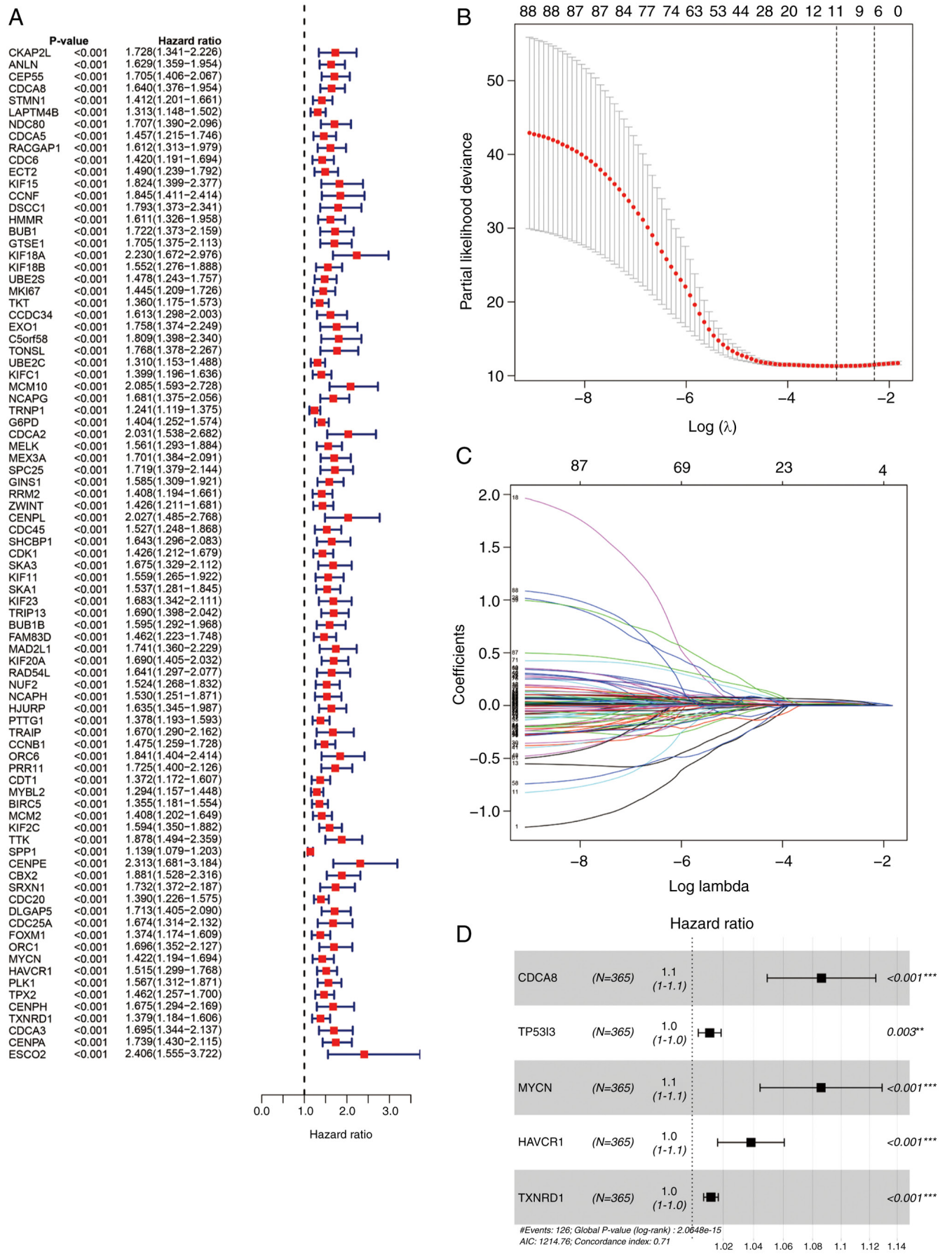

Figure 3. Establishment of CRG signature. (A) Univariate Cox regression analysis identified 88 prognosis-related CRGs. LASSO Cox regression analysis excluded relatively insignificant parameters. (B) Plot of partial likelihood deviance vs. log(l) for the LASSO regression model. (C) Plot of coefficients vs. log(l) for the LASSO regression model. (D) Five signature genes were identified by multivariate Cox regression. **P<0.01 and ***P<0.001. CRG, circulating tumor cell/circulating tumor microemboli-related gene; LASSO, least absolute shrinkage and selection operator; AIC, Akaike information criterion.

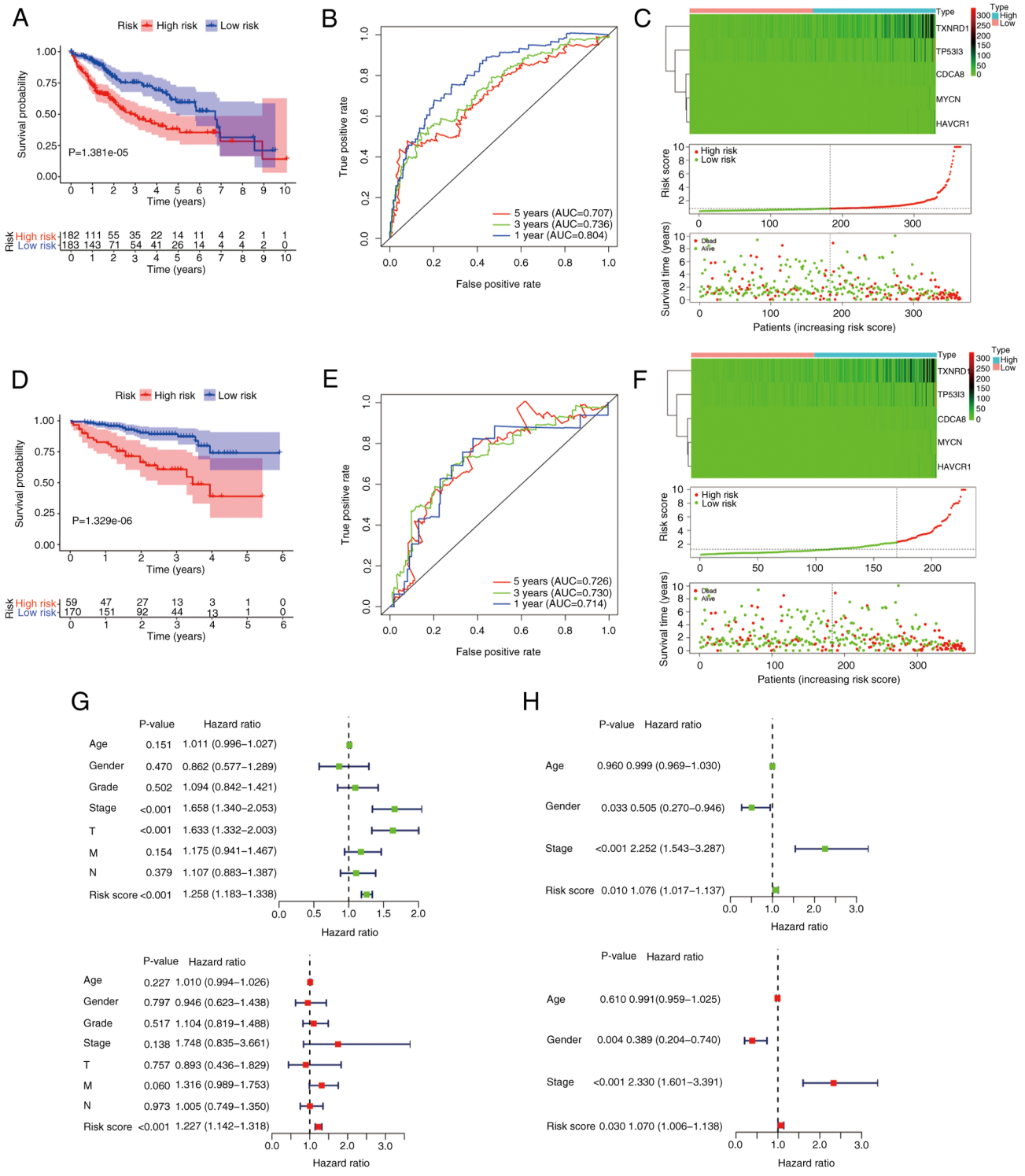

Figure 4. Predictive efficiency validation of the prognosis signature. (A) OS curves of patients in the low- and high-risk groups in TGCA cohort (analyzed using the 2-stage test). (B) ROC curves for 1-, 3- and 5-year survival in TCGA cohort. (C) Distribution pattern of the expression of model genes (upper), risk score delamination (middle) and survival state (lower) in the TGCA cohort. (D) OS analysis, (E) time-dependent ROC analysis and (F) distribution pattern of expression of model genes (upper), risk score delamination (middle) and survival state (lower) in the ICGC cohort. (G and H) Univariate analysis (upper) and multivariate (lower) analysis of prognostic factors for OS in the (G) TCGA and (H) ICGC cohorts. OS, overall survival; TCGA, The Cancer Genome Atlas; ROC, receiver operating characteristic; ICGC, International Cancer Genome Consortium; AUC, area under the curve.

Validation of the signature in the GEO cohort. To further verify the predictive power of the prognostic signature, the GSE14520 dataset was analyzed. In this dataset, 221 valid patients were included, with 100 in the high-risk group and 121 in the low-risk group. As the results in Fig. 5A illustrate, patients in the low-risk group had improved survival outcomes compared with those in the high-risk group (P<0.05). In the GEO cohort, the AUC for 5-year OS was 0.684 (Fig. 5B). The expression of model genes, risk score distribution and survival status for each patient in this validation cohort are

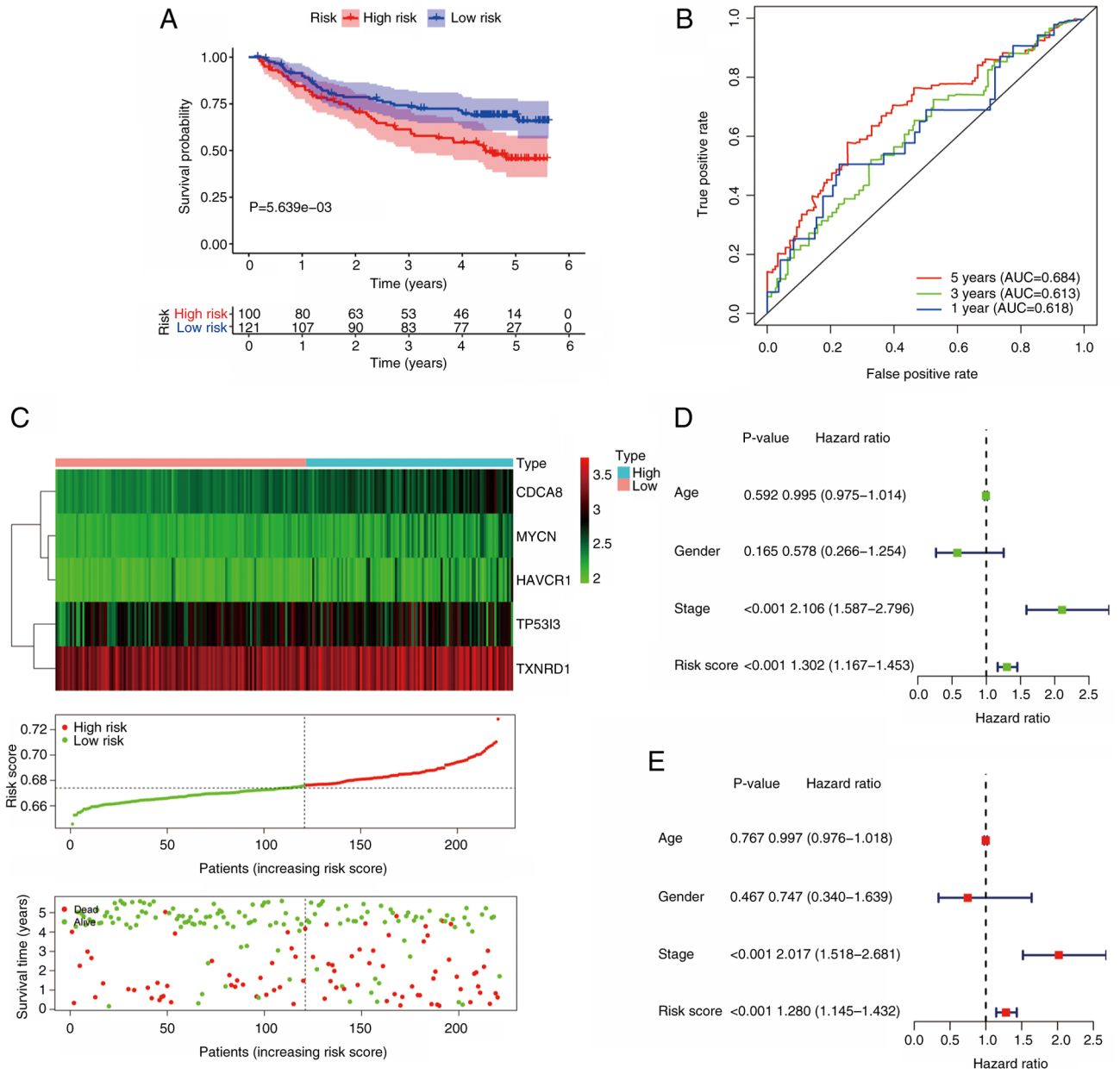

Figure 5. Validation of the signature in the GEO cohort GSE14520. (A) OS curves of patients in the low- and high-risk groups. (B) Receiver operating characteristic curves of patients with liver cancer at 1, 3 and 5 years. (C) Expression pattern of model genes (upper), risk score delamination (middle) and survival state in the cohort. (D) Univariate and (E) multivariate analysis of prognostic factors for OS in the GEO cohort. GEO, Gene Expression Omnibus; OS, overall survival; AUC, area under the curve.

shown in Fig. 5C. Following univariate Cox regression analysis (Fig. 5D), the results of independent prognostic analysis revealed that risk score (P<0.001; HR=1.280; 95% CI, 1.145-1.432), as well as AJCC stage (P<0.001; HR, 2.017; 95% CI, 1.518-2.681) (Fig. 5E) were independent risk factors in this cohort. These findings indicate that the prognostic model is promising as a predictive signature.

Identification of CTC/CTM-related molecular subtypes. Patients were clustered into different subtypes based on the expression levels of the five prognostic signature genes using the NMF algorithm. To ensure the robustness of the clustering results, the coefficient of correlation was used to determine the optimal number of clusters, and when the number of clusters was 2, clear boundaries were observed for both subtypes. This indicated the stable and reliable clustering of the liver cancer samples (Fig. 6A). The OS of patients in cluster 1 (C1) was significantly improved compared with that of C2 (P=0.002; Fig. 6B). Most immune checkpoints were upregulated in the C2 group compared with the C1 group (Fig. 6C). In addition, it was also found that the level of immune infiltration in the tumor microenvironment was also distinct in the two groups, with immune score, stromal score and ESTIMATE score of the C1 group being significantly lower than those of the C2 group (P<0.05; Fig. 6D). This suggests that C1 molecular subtype tends to present 'cold tumors', whereas the C2 molecular subtype tends to present 'hot tumors'. It was also noted that the level of neutrophil infiltration was higher in the C1 group than

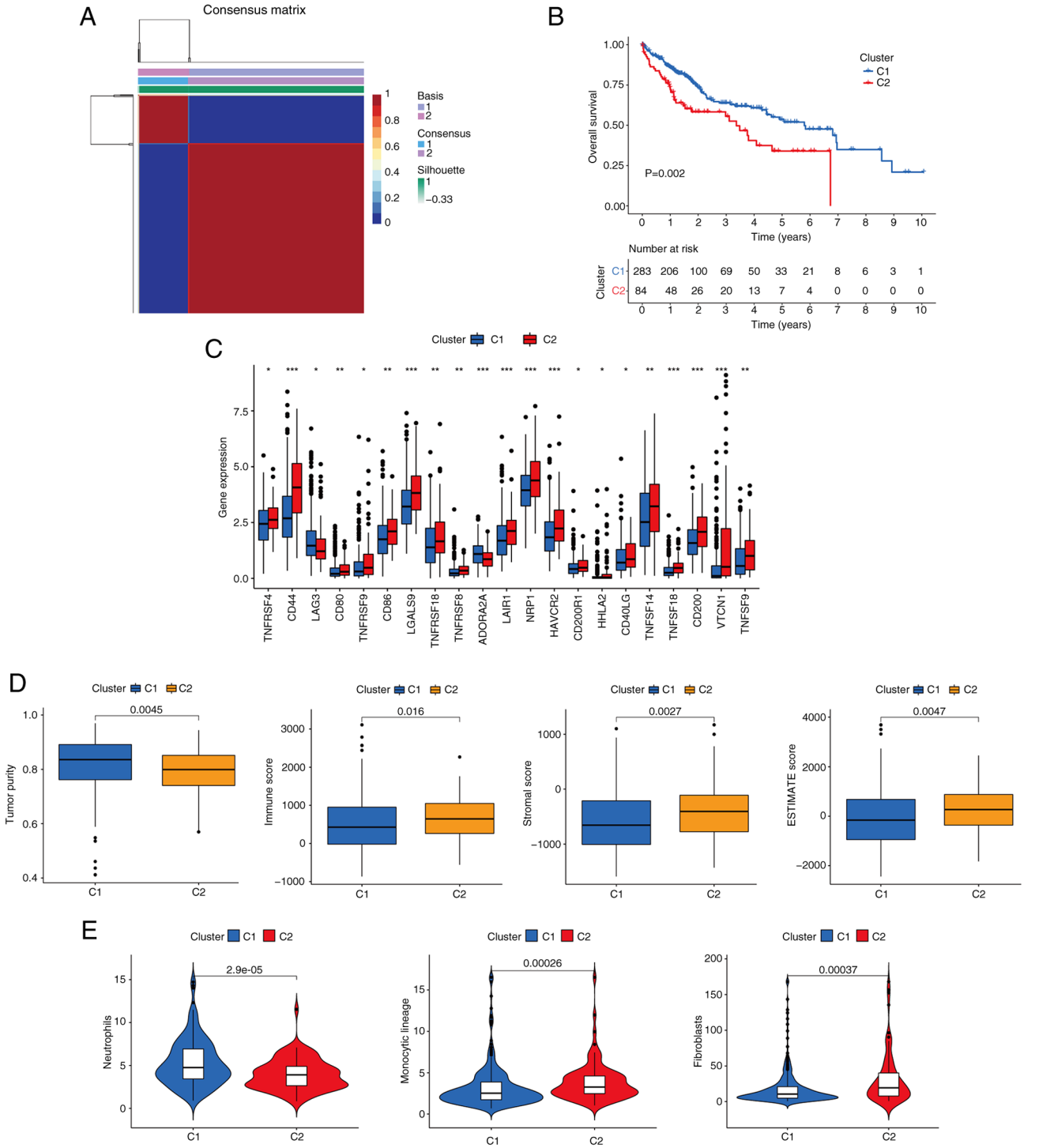

Figure 6. Construction of molecular subtypes of liver cancer. (A) Consensus map of liver cancer via the NMF algorithm. (B) Kaplan-Meier survival curve for overall survival of the C1 and C2 patient subgroups. (C) Expression of immune checkpoints between patients with type C1 and C2 cancers. (D) Comparison of tumor purity, immune score, stromal score, and ESTIMATE score between the two NMF types. (E) Enrichment scores of neutrophils, monocytic lineage and fibroblasts between type C1 and C2 patients. *P<0.05, **P<0.01 and ***P<0.001. NMF, non-negative matrix factorization.

in the C2 group, whereas the levels of monocytic lineage and fibroblast infiltration were lower in the C1 group than in the C2 group (P<0.05; Fig. 6E).

Identification of potentially therapeutic small molecule drugs. The sensitivity of the high- and low-risk groups to various chemotherapeutic agents was compared to evaluate drugs for potential use in liver cancer. The findings indicate that the low-risk group was associated with a higher IC_{50} for chemotherapeutic compounds including ABT.888 (veliparib), AS601245 (an ATP-competitive JNK inhibitor), AG.014699 (rucaparib), A.443654 (a pan-Akt inhibitor), ATRA (tretinoin) and AUY922 (luminespib). By contrast, axitinib, A.770041 (an LCK inhibitor), AZD.0530 (saracatinib), AMG.706 (motesanib), AKT.inhibitor.VIII and AICAR (acadesine) had a higher IC_{50} in the high-risk group, indicating that patients

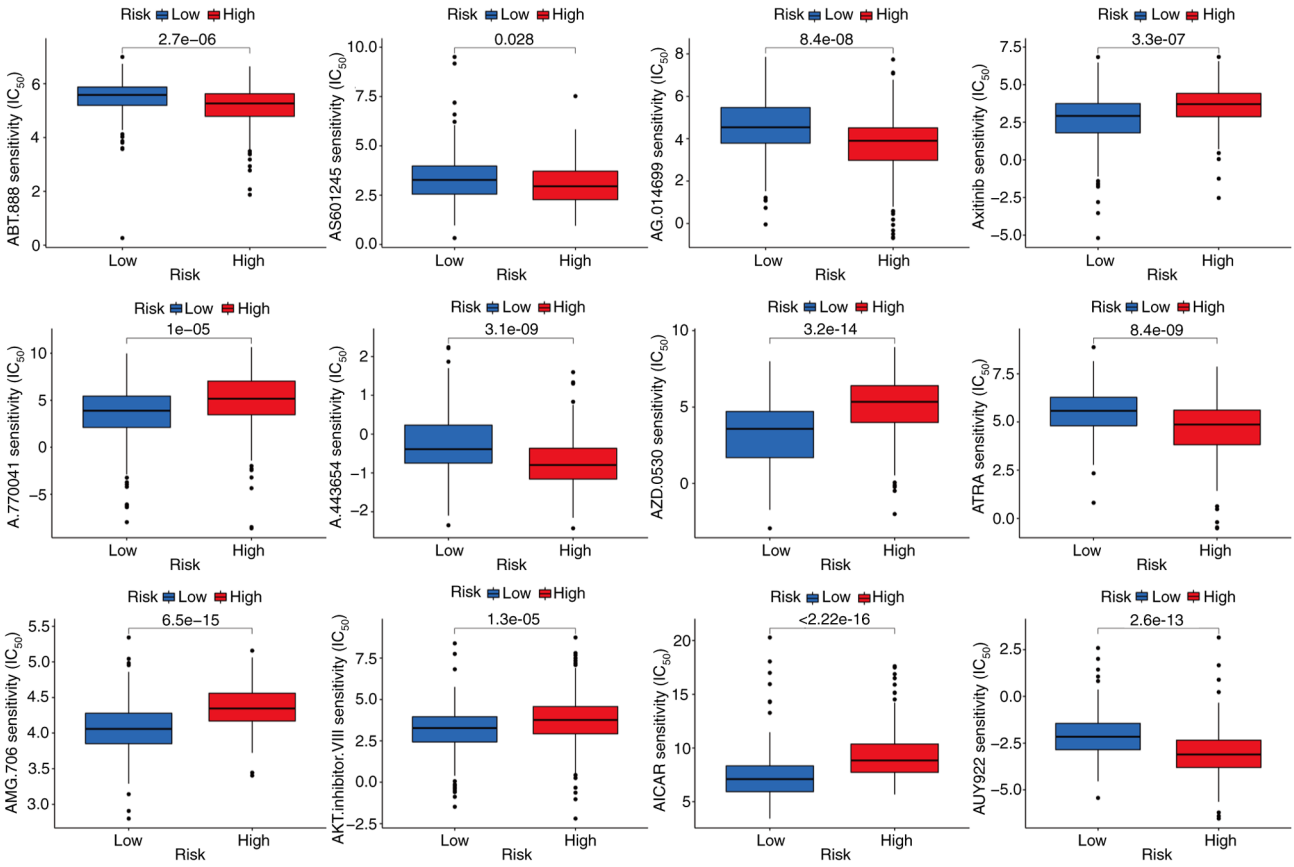

Figure 7. IC_{50} analysis of cytotoxic chemotherapeutic agents in high- and low-risk liver cancer groups. IC_{50}, half-maximal inhibitory concentration.

in the low-risk group may benefit more from treatment with these compounds (P<0.05; Fig. 7). The sensitivity of the two liver cancer subtypes to various chemotherapeutic drugs was also evaluated. The results suggested that patients with the C1 subtype might be more sensitive to metformin, lapatinib, elesclomol, docetaxel, camptothecin, bosutinib, axitinib and vinblastine, while patients in group C2 would likely benefit by treatment with cisplatin, bortezomib, bleomycin, bicalutamide, mitomycin C, imatinib, etoposide and gemcitabine (Fig. S1).

Pathway analysis by GSEA and GSVA. To further explore the molecular mechanism associated with the signature genes and the prognostic module, GSEA was performed in TCGA liver cancer cohort. Fig. 8A-E reveals the KEGG pathways of the five signature genes, namely CDCA8, HAVCR1, MYCN, TP53I3 and TXNRD1, showing the five most upregulated and downregulated pathways for each gene. The signature genes are mainly concentrated in KEGG pathways including 'cell cycle', 'p53 signaling pathway', 'complement and coagulation cascades' and 'drug metabolism cytochrome p450'. In addition, GSEA was used to compare the high- and low-risk groups based on the risk scores. The KEGG pathways enriched in the high and low risk groups are shown in Fig. 8F.

GSVA was also utilized to analyze the differences in biological behavior between the high- and low-risk groups. The results demonstrated that pathways associated with tumor progression, such as 'cell cycle', 'DNA replication', 'RNA degradation', 'mTOR signaling pathway' and 'P53 signaling pathway', were mainly concentrated in the high-risk group. By contrast, metabolism-related pathways, including 'fatty acid metabolism', 'propanoate metabolism', 'butanoate metabolism' and 'tyrosine metabolism', were mainly present in the low-risk group of patients (Fig. 8G).

Differentiation of immune infiltration between the two risk subgroups. In view of the important role of immune checkpoints in tumor immunotherapy, the differential expression of immune checkpoint genes was analyzed between risk subgroups. The results revealed that common immune checkpoint genes, including cytotoxic T-lymphocyte associated protein 4 (CTLA4), CD274, programmed cell death 1, and T-cell immunoreceptor with Ig and ITIM domains were upregulated in the high-risk group compared with the low-risk group (P<0.05; Fig. 9A). This suggests that the poor prognosis of high-risk patients with liver cancer may at least partially be attributed to an immunosuppressive microenvironment. Chemokines and their receptors are necessary for the targeted migration of immune cells and the initiation and execution of the immune response (45,46). Therefore, the differential expression of chemokines and their receptors was analyzed in the two risk subgroups, which revealed higher levels of expression for the majority of these chemokines and receptors in patients in the high-risk group (P<0.05; Fig. 9B and C). An association between risk score and HLA-associated gene expression was also observed. As shown in Fig. 9D, the abundance of HLA-related genes was higher in patients at high risk than those in the low-risk group (P<0.05). The results of algorithms were visualized using heat maps, including assessment

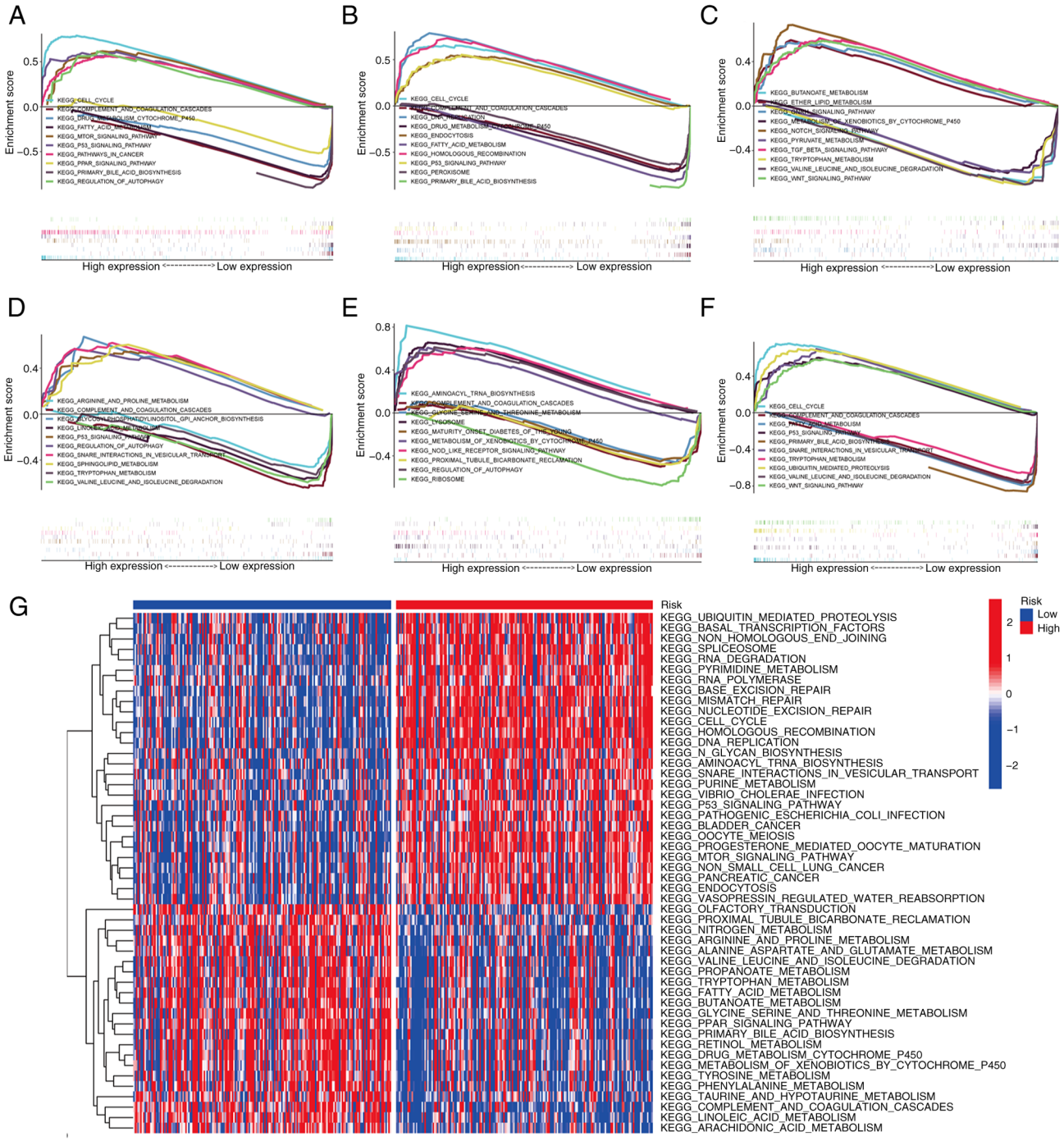

Figure 8. GSEA of signature genes and risk groups and pathways identified by GSVA. GSEA analysis for (A) cell division cycle associated 8, (B) hepatitis A virus cellular receptor 1, (C) MYCN proto-oncogene, (D) tumor protein p53 inducible protein 3 and (E) thioredoxin reductase 1. (F) GSEA analysis between low- and high-risk groups in The Cancer Genome Atlas cohort. Each analysis includes five upregulated and five downregulated pathways. (G) Heatmap illustrating the different biological pathways of the GSVA. GSEA, gene set enrichment analysis; GSVA, gene set variation analysis.

of immune cell infiltration in the two risk subgroups, and the results suggest that the high-risk group has more abundant immune cell infiltration (Fig. 9E). In addition, further exploration of the association between risk score and immune pathway activity revealed that cytolytic activity, type I IFN response and type II IFN response scores were higher in the low-risk group, and conversely, the MHC class I score was higher in the high-risk group (P<0.05; Fig. 10F). These results demonstrate that patients in the high-risk group are more likely to benefit from immunotherapy.

Clinicopathological parameter correlation analysis. To investigate the prognostic value of the CRG signature in patients with different clinical features, a heat map was drawn to reveal whether there was a potential association with clinicopathological features in the high- and low-risk subgroups (Fig. 10A). The expression levels of CDCA8 and TXNRD1 were higher in the high-risk group than in the low-risk group. In addition, the results revealed that the high-risk score was closely associated with a higher T stage (P<0.001), higher grade (P<0.001), higher tumor stage (P<0.001) and poor patient survival status (P<0.001).

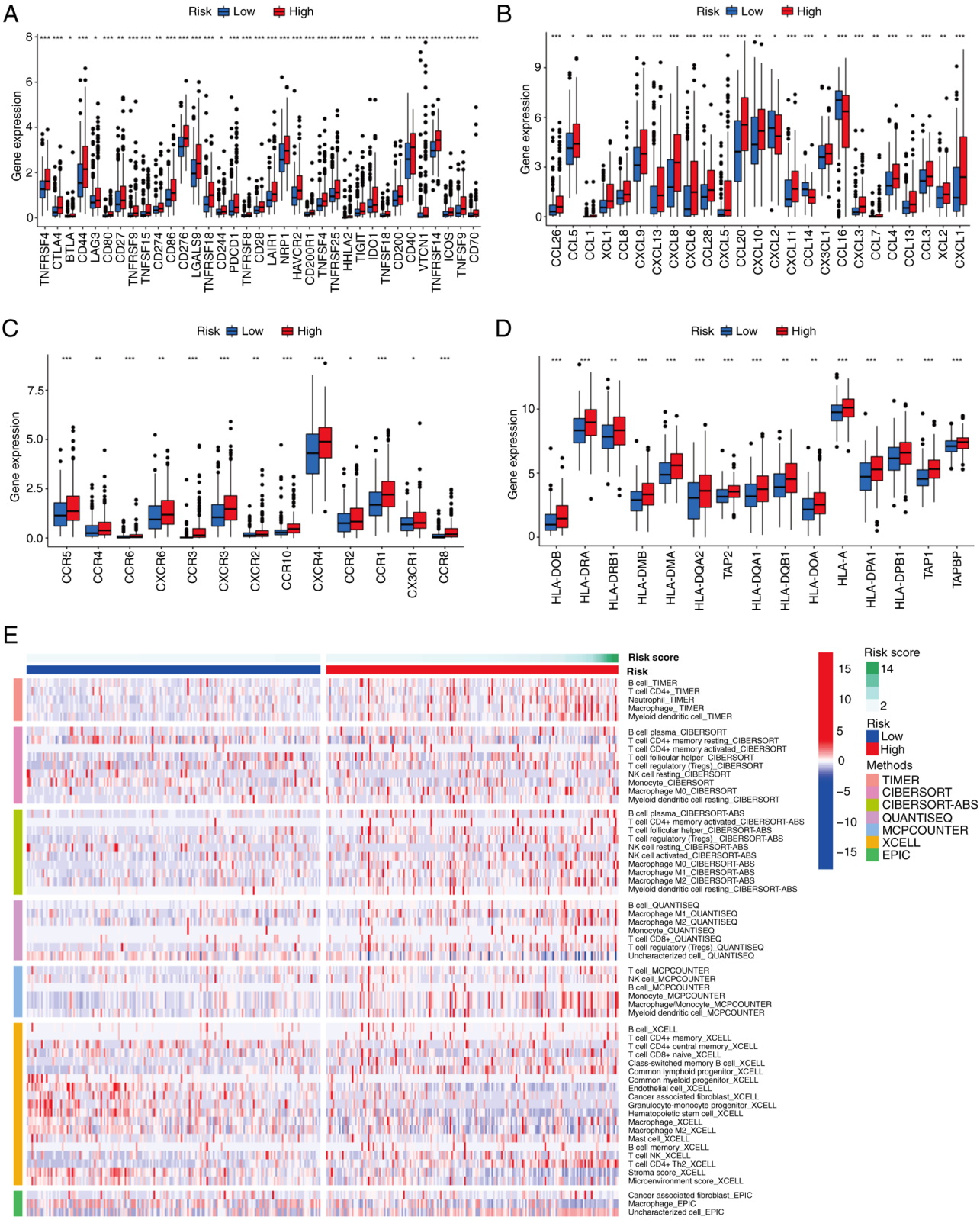

Figure 9. Immune checkpoints, chemokines, chemokine receptors, HLA-related molecules and immune infiltration for different risk stratifications. Differential expression of (A) immune checkpoint genes, (B) chemokines, (C) chemokine receptors and (D) HLA-related molecules between the low- and high-risk groups. (E) Correlation of risk scores and immune cell infiltration was analyzed through multiple immune infiltration algorithms. *P<0.05, **P<0.01 and ***P<0.001. HLA, human leukocyte antigen.

Analysis of the immunological value of the CRG signature. Since TMB and tumor immune dysfunction and exclusion (TIDE) are good indicators of the response to immunotherapy, sample scores were calculated for each patient with liver cancer and variability between the high- and low-risk subgroups was assessed. The results revealed that the high-risk group had

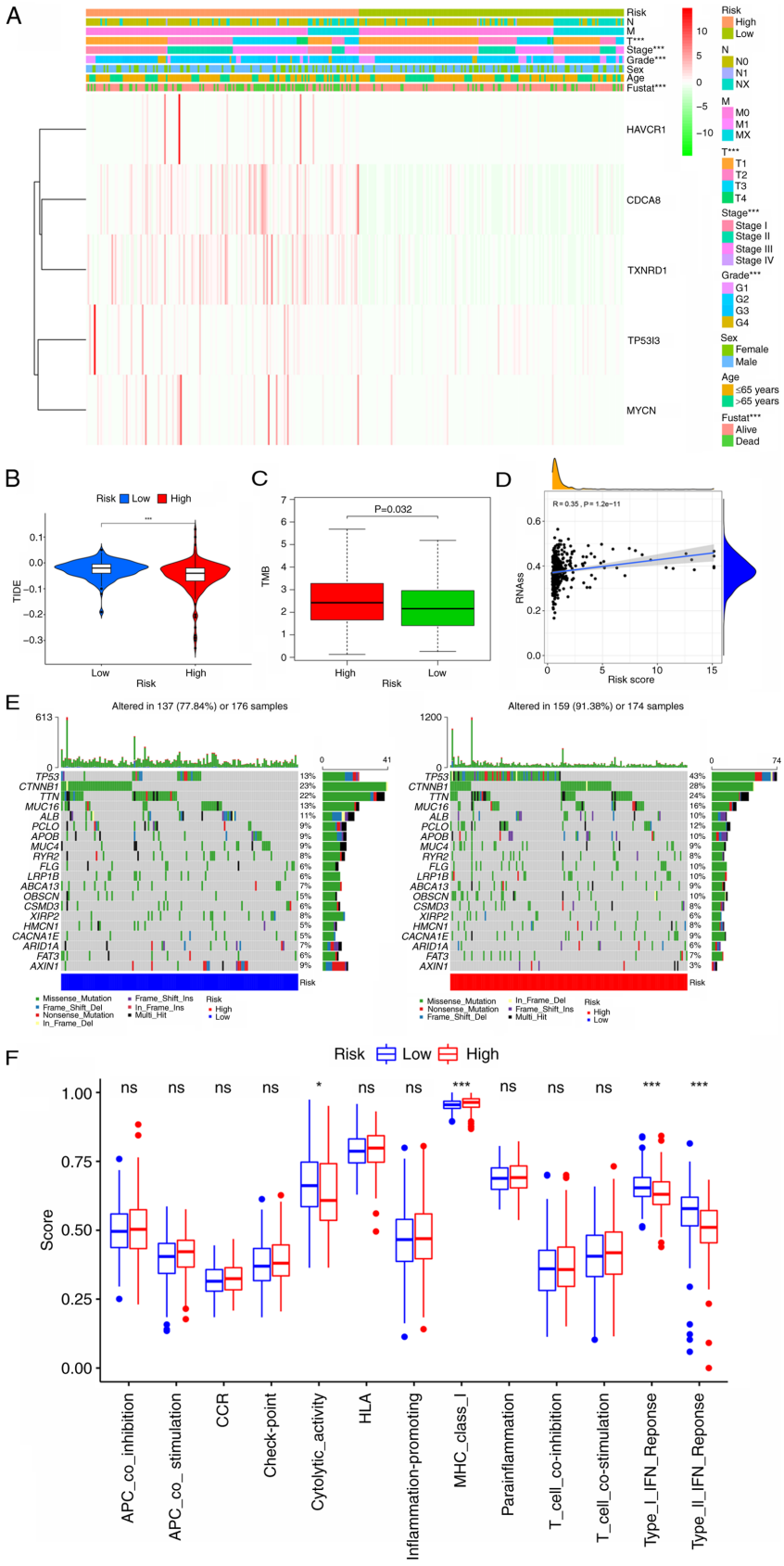

Figure 10. Analysis of the clinical utility of the CRG signature and comparison of TIDE, TMB, stem cell content, the frequency of mutations and immune signaling pathways between the high- and low-risk groups. (A) Heatmap showing the correlation of the prognostic signature with clinicopathological characteristics and five signature genes. (B and C) Boxplots showing the difference in (B) TIDE and (C) TMB between the low- and high-risk CRG groups. (D) Correlation between RNAss and the risk score. (E) Mutation rate analysis of the two risk groups. (F) Comparison of scores for immune-related pathways between the high- and low-risk groups. *P<0.05 and ***P<0.001. CRG, circulating tumor cell/circulating tumor microemboli-related gene; TIDE, tumor immune dysfunction and exclusion; TMB, tumor mutation burden; RNAss, RNA stemness score; fustat, follow-up status; HAVCR1, hepatitis A virus cellular receptor 1; CDCA8, cell division cycle associated 8; TXNRD1, thioredoxin reductase 1; TP53I3, tumor protein p53 inducible protein 3; MYCN, MYCN proto-oncogene; ns, not significant.

a higher TMB and lower TIDE index, which further demonstrates that patients in the high-risk group should be more responsive to immunotherapy (P<0.05; Fig. 10B and C). The mRNA expression-based stemness score revealed a positive correlation between liver cancer tumor stemness and the risk score, indicating that tumors in the high-risk group are more likely to undergo malignant progression and thus lose their differentiated phenotype (P<0.05; Fig. 10D). In addition, the maftools R package was used to visualize the differences in somatic mutation distribution between the high- and low-risk groups. The results demonstrated that the high-risk group had a higher mutation frequency compared with the low-risk group (91.38 vs. 77.84%, respectively). The most mutated gene in the low-risk group was catenin b1 (23%) and the most mutated gene in the high-risk group was TP53 (43%) (Fig. 10E).

Correlation analysis of risk signature genes and immune checkpoints. Immune checkpoints have an important role in immune regulation, and immune checkpoint inhibitors are used in cancer therapy. Therefore, the associations between the signature genes and the expression of immune checkpoint genes, namely programmed cell death protein 1 (PD-1), programmed death-ligand 1 (PD-L1) and CTLA4, were investigated. The results in Fig. 11A indicate that the expression of CDCA8 was positively correlated with that of the three immune checkpoints, PD-1 (R=0.3; P=$4.9x10^{-9}$), PD-L1 (R=0.32; P=$3.8x10^{-10}$) and CTLA4 (R=0.32; P=$3.9x10^{-10}$). In addition, the expression of HAVCR1 was positively correlated with CTLA4 expression (R=0.32; P=$1.3x10^{-10}$). TISIDB portal was used to analyze the expression of signature genes in different immune subtypes, specifically: C1, wound healing; C2, IFN-g dominant; C3, inflammatory; C4, lymphocyte depleted; C5, immunologically quiet; and C6, TGF-b dominant (47). The results indicated that the roles of these five genes differ among the different immune subtypes, with CACA8, MYCN and TXNRD1 being differentially expressed among the immune subtypes. Specifically, the TISIDB analysis revealed that CDCA8 was highly expressed in the C1 and C2 types, MYCN was highly expressed in the C1 type, and TXNRD1 was mainly expressed in the C2 and C4 types (Fig. 11B). In addition, the IMvigor dataset was used to predict the responsiveness of the five signature genes to atelelizumab treatment. Notably, consistent with the previous findings, the analysis suggested that patients with high expression of CDCA8 and TXNRD1 may obtain improved treatment outcomes (Fig. 11C). The correlations between tumor immune infiltration by $CD4^+$ T cells, $CD8^+$ T cells, B cells, neutrophils, macrophages and dendritic cells, and the expression of the five signature genes were also investigated (Fig. S2). In this analysis, correlation coefficients >0.3 and P<0.05 were considered as distinctive; partial.cor denotes partial correlation, indicating the correlation of gene expression with immune cell infiltration in the TIMER database. The results show that CDCA8 expression is positively correlated with the infiltration of six types of immune cells: B cells (partial.cor, 0.441; P=$9.08x10^{-18}$), $CD8^+$ T cells (partial.cor, 0.303; P=$1.03x10^{-8}$), $CD4^+$ T cells (partial.cor, 0.359; P=$6.74x10^{-12}$), macrophages (partial.cor, 0.439; P=$1.70x10^{-17}$), neutrophils (partial.cor, 0.368; P=$1.63x10^{-12}$) and dendritic cells (partial.cor, 0.465; P=$1.22x10^{-19}$). Similarly, HAVCR1 expression was found to be positively correlated with the infiltration of B cells (partial.cor, 0.302; P=$1.14x10^{-8}$), macrophages (partial.cor, 0.302; P=$1.34x10^{-8}$), neutrophils (partial.cor, 0.392; P=$4.00x10^{-14}$) and dendritic cells (partial.cor, 0.317; P=$2.18x10^{-9}$), and TXNRD1 expression was positively associated with neutrophil infiltration (partial.cor, 0.322; P=$8.67x10^{-10}$).

Comparison of the CRG signature with external prognostic models. To better assess the predictive efficacy of the CRG prognostic model, the risk signature was compared with six published liver cancer prognostic models. The signature of Du *et al* (48) was a m6A-based gene signature; the signature of Fu and Song (49) was a pyroptosis-related gene signature; the signature of Guo *et al* (50) was a signature containing nine genes; Lei *et al* (51) devised a starvation-based nine-mRNA signature; Tian *et al* (52) proposed a five-gene prognostic signature for liver cancer; and the signature of Zheng *et al* (53) comprised five pyroptosis-related genes. When the accuracy of these models and the current model were compared, it was found that the C-index and restricted mean survival of the CRG signature were higher than those of the other six models, which indicates that the present model is optimal (Fig. 12A and B). Additionally, the AUCs of the CRG model for 1-, 3- and 5-year OS were 0.807, 0.711 and 0.667, respectively, which were higher than those of the other signatures, which validates the previous results (Fig. 12C).

Establishment and validation of a predictive nomogram. To forecast the survivability of patients with liver cancer, a nomogram including factors such as age, sex, stage and risk score was created to predict probability of OS at 1, 3, and 5 years in the TCGA cohort. In addition, calibration plots were constructed to evaluate the predictive power of the nomogram (Fig. 12D). Similarly, two nomograms were also constructed for the ICGC and GSE14520 cohorts (Fig. S3). These all indicate the good predictive power of the model.

Downregulation of TP53I3 inhibits liver cancer cell proliferation. Among the five signature genes, CDCA8, MYCN, HAVCR1 and TXNRD1 have previously been demonstrated to have a biological regulatory function in liver cancer (*vide infra*), but TP53I3 has been poorly studied in liver cancer. Therefore, the role of TP53I3 in liver cancer cells was evaluated using cellular experiments. TP53I3 was knocked down in HepG2 and MHCC97H cells using siRNA, and the transfection efficiency was verified by western blot analysis and RT-qPCR (Fig. 13A and B). To explore the impact of TP53I3 on the proliferation of liver cancer cells *in vitro*, CCK-8, EdU and colony formation analyses were performed. The results showed that the proliferation ability and colony formation of the liver cancer cells was significantly suppressed after TP53I3 depletion (P<0.05; Fig. 13C-E), which indicates that TP53I3 promotes the proliferation of liver cancer cells.

Discussion

Liver cancer remains a significant challenge to human health, with high rates of incidence and recurrence, even after surgical resection. Numerous studies have demonstrated that CTCs are

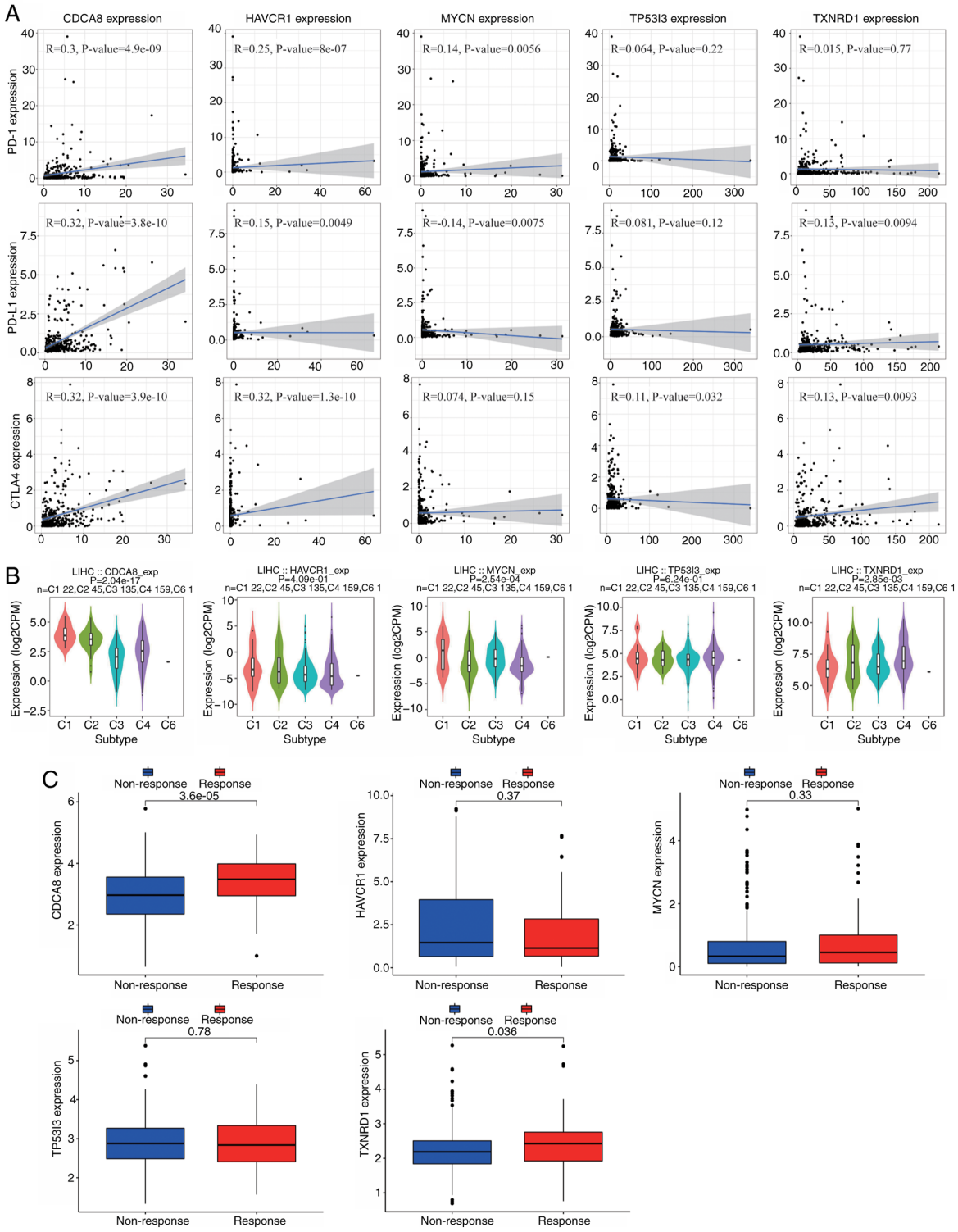

Figure 11. Correlation analysis of five CRGs and immunity markers. (A) Correlation between CRGs and the immune checkpoints PD-1, PD-L1 and CTLA4. (B) Analysis of the role of the five CRGs in different immune subtypes. (C) Expression levels of the five CRGs in the IMvigor210 cohort. CRGs, circulating tumor cell/circulating tumor microemboli-related genes; PD-1, programmed cell death protein 1; PD-L1, programmed death-ligand 1; CTLA4, cytotoxic T-lymphocyte associated protein 4; CDCA8, cell division cycle associated 8; HAVCR1, hepatitis A virus cellular receptor 1; MYCN, MYCN proto-oncogene; TP53I3, tumor protein p53 inducible protein 3; TXNRD1, thioredoxin reductase 1; LIHC, liver hepatocellular carcinoma; exp, expression; CPM, counts per million reads.

tightly associated with the metastasis, epithelial-mesenchymal transition and recurrence of malignant tumors, including liver cancer (54-58). Therefore, it is critical to screen molecules associated with CTCs to identify biomarkers for the prediction of liver cancer. In the present study, a reliable prognostic signature based on CRGs was constructed and its clinical application in patients with liver cancer was explored. The results showed that the CRG prognostic model accurately predicted the prognosis and immunotherapy sensitivity of patients with liver cancer.

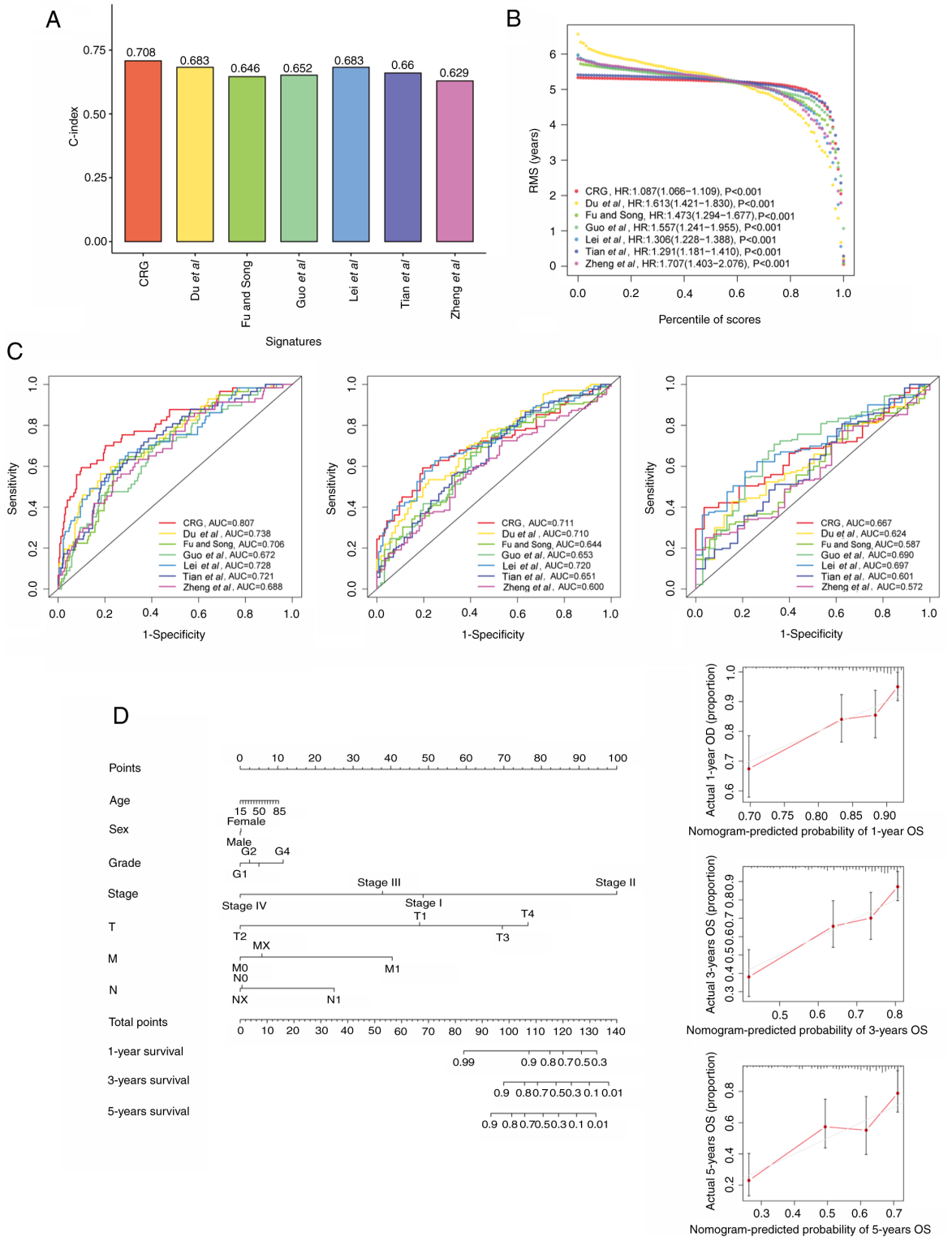

Figure 12. Verification of the superiority of the CRG signature compared with six previously reported signatures. (A) C-index and (B) RMS curves for the seven risk signatures. (C) Receiver operating characteristic curves and AUCs for 1-, 3- and 5-year survival predication by the seven signatures. (D) Nomogram and calibration curves for prediction of the 1-, 3-, and 5-year survival of patients with liver cancer in The Cancer Genome Atlas cohort. CRG, circulating tumor cell/circulating tumor microemboli-related gene; RMS, restricted mean survival; HR, hazard ratio; AUC, area under the curve; OS, overall survival.

In the present study, 258 CRGs were identified by systematically analyzing the DEGs in TCGA and ICGC databases and the CTC expression profiles of liver cancer. These genes were then screened to construct a five-CRG signature in the TCGA cohort. Kaplan-Meier survival and ROC analyses were performed to confirm the prognostic value of the signature, and the results were validated in ICGC and GEO cohorts. Univariate and multifactorial Cox analyses further confirmed that the risk signature was able to serve as an independent prognostic factor. In addition, nomograms for all three cohorts showed the good predictive power of the model. The genes in the prognostic signature were CDCA8, HAVCR1, TP53I3, MYCN and TXNRD1,

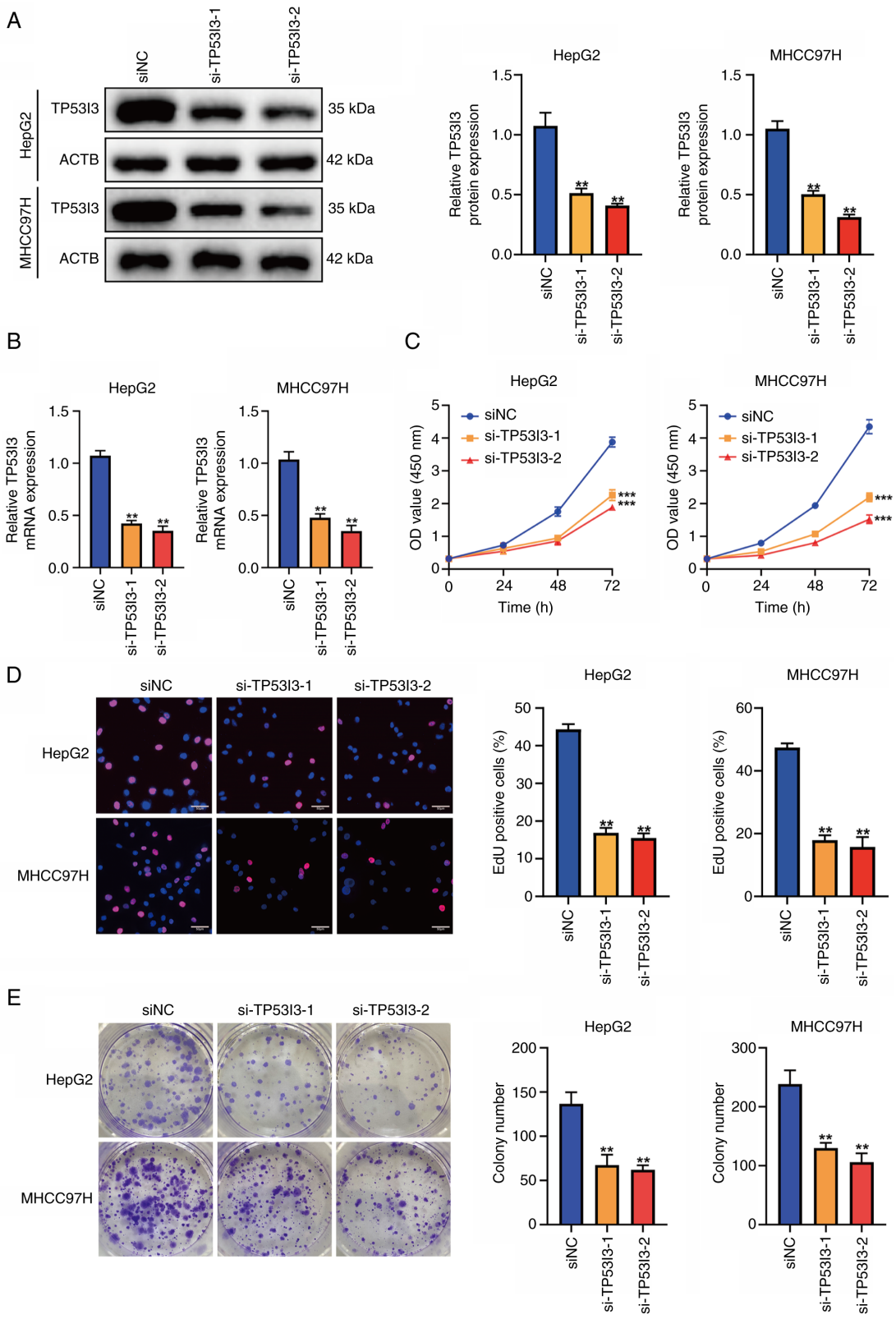

Figure 13. Silencing TP53I3 inhibits the proliferation of liver cancer cells *in vitro*. (A) Western blotting and (B) reverse transcription-quantitative polymerase chain reaction analyses showed that TP53I3 was stably knocked down in HepG2 and MHCC97H cells. (C) Cell Counting Kit-8, (D) EdU (scale bar, 50 μm) and (E) colony formation assays were performed to analyze the proliferation and colony formation of the liver cancer cells after TP53I3 knockdown. Data are presented as the mean ± SD; n=3. **P<0.01 and ***P<0.001 vs. siNC. TP53I3, tumor protein p53 inducible protein 3; si, small interfering RNA; siNC, negative control siRNA; OD, optical density; EdU, 5-ethynyl-2'-deoxyuridine.

all of which have the potential to be used as liver cancer prognostic risk genes. Previous studies have demonstrated the ability of CDCA8 to promote cancer cell proliferation and migration in several tumors, including esophageal squamous cell carcinoma (59), thyroid cancer (60), malignant glioma and cutaneous melanoma (61). In addition, Jeon *et al* (62) demonstrated that

silencing CDCA8 effectively suppressed liver cancer growth and stemness, implying that CDCA8 may be a CTC-related gene. HAVCR1 is highly expressed in a variety of tumors, including colorectal cancer, non-small-cell lung cancer, clear cell renal cell carcinoma and liver cancer, and is an independent prognostic factor (63-66). Moreover, Ye *et al* (66) found that T-cell immunoglobulin mucin-1$^+$ (HAVCR1$^+$) regulatory B cell infiltration was significantly higher in liver tumor tissues compared with paraneoplastic tissues in patients with liver cancer and promoted the immune escape of liver cancer cells, implying that it could be used as an immune therapeutic target. TP53I3, also known as p53-inducible gene 3, is involved in the apoptosis process and DNA damage response. Previous studies have revealed that TP53I3 promotes the invasion and metastasis of lung cancer cells and that silencing TP53I3 increases the chemosensitivity of non-small cell lung cancer cells to docetaxel (67,68). Notably, the present study also demonstrated that the knockdown of TP53I3 inhibited the proliferation ability of liver cancer cells in cellular experiments. These findings may indicate a novel strategy for the treatment of liver cancer. Qin *et al* (69,70) highlighted that MYCN, a member of the MYC proto-oncogene family, may be a stem cell-like marker for liver cancer and is potentially a therapeutic target of acyclic retinoid for liver cancer. TXNRD1 is an antioxidant enzyme that has been reported to be overexpressed in liver cancer. Lee *et al* (71) observed that the inhibition of TXNRD1 suppressed liver cancer cell proliferation, promoted apoptosis and induced oxidative stress, suggesting that it could be used as a therapeutic target for liver cancer. In conclusion, these previous studies suggest that the five signature genes have an important role in the development of liver cancer and may have potential as therapeutic targets.

As indicated by KEGG analysis, CRGs may promote the development, metastasis and recurrence of liver cancer via the cell cycle and p53 signaling pathway. GSEA analysis of the five signature genes and the high-risk group in the prognostic model identified various oncogenesis-associated features, including the terms 'cell cycle', 'p53 signaling pathway', 'WNT signaling pathway' and 'DNA replication'. In addition, GSVA results showed that tumor progression-related pathways, such as 'cell cycle', 'DNA replication', 'mTOR signaling pathway' and 'P53 signaling pathway', were mainly concentrated in the high-risk group, which was generally consistent with the GSEA results. On the basis of this, a number of potential therapeutic agents were also evaluated, with veliparib (72), ATRA (73,74) and AUY922 (75) exhibiting high drug sensitivity in the high-risk group, suggesting that these agents are likely to be therapeutic candidates.

Immunotherapy is playing an increasingly important role in liver cancer. Therefore, the relevance of the present model to immune infiltration and immunotherapy was also analyzed in the present study. Immune cell infiltration analysis demonstrated that CDCA8 and HAVCR1 correlated with the infiltration abundance of several immune cells, including B cells, CD8$^+$ T cells, macrophages, neutrophils and dendritic cells. In addition, immune checkpoint expression, TMB scores and immune cell infiltration levels were strongly associated with patients in the high-risk subgroup. The analysis of somatic mutation rates also indicated that patients in the high-risk group had an elevated frequency of mutations and greater occurrence of TP53 mutations. It has been proposed that TIDE scores may be used by oncologists to assist in the selection of suitable patients for immune checkpoint inhibition therapy (76). Consistent with this, the present study found that patients in the high-risk group had lower TIDE scores, while those in the low-risk group had higher TIDE scores, indicating that the high-risk patients may benefit more from immunotherapy. All these findings confirm that the present model has good risk stratification capabilities and is suitable for selecting the patients who may benefit from immunotherapy.

Notably, this five-risk gene signature was also used to identify liver cancer subgroups C1 and C2, of which C2 as a high-risk subgroup showed a worse prognosis. Compared with group C1, group C2 had a higher immune checkpoint expression and higher stromal, immune and ESTIMATE scores for each sample, which also suggested that patients in group C2 were more suitable for immunotherapy. More importantly, several chemotherapeutic agents to which C2 patients should be sensitive were also identified. These were cisplatin (77), bortezomib (78), bleomycin, bicalutamide, mitomycin C, imatinib, etoposide and gemcitabine (79), which could improve the prognosis of patients in the C2 group. In conclusion, the findings of this analysis are helpful, but future studies are necessary to verify this.

However, the study has some limitations. For example, the regulatory role of these five CRGs in liver cancer were not further investigated experimentally. Other external validation of the model is lacking and must to be conducted in clinical samples in the future. In addition, chemotherapy were not analyzed. Therefore, additional studies and more evidence are required to refine the present model in the future.

Acknowledgements

Not applicable.

Funding

Not applicable.

Availability of data and materials

The data generated in the present study may be requested from the corresponding author.

Authors' contributions

LX was responsible for conceptualization, methodology, software and writing the original draft of the manuscript. QW performed validation, and reviewed and edited the manuscript. KZ, XL and WY performed data analysis and interpretation. XL and WY confirm the authenticity of all the raw data. All authors read and approved the final version of the manuscript.

Ethics approval and consent to participate

Not applicable.

Patient consent for publication

Not applicable.

Competing interests

The authors declare that they have no competing interests.

References

1. Global Burden of Disease Cancer Collaboration; Fitzmaurice C, Allen C, Barber RM, Barregard L, Bhutta ZA, Brenner H, Dicker DJ, Chimed-Orchir O, Dandona R, *et al*: Global, regional, and national cancer incidence, mortality, years of life lost, years lived with disability, and disability-adjusted life-years for 32 cancer groups, 1990 to 2015: A systematic analysis for the global burden of disease study. JAMA Oncol 3: 524-548, 2017.
2. Villanueva A: Hepatocellular carcinoma. N Engl J Med 380: 1450-1462, 2019.
3. Sung H, Ferlay J, Siegel RL, Laversanne M, Soerjomataram I, Jemal A and Bray F: Global cancer statistics 2020: GLOBOCAN estimates of incidence and mortality worldwide for 36 cancers in 185 countries. CA Cancer J Clin 71: 209-249, 2021.
4. Llovet JM, Kelley RK, Villanueva A, Singal AG, Pikarsky E, Roayaie S, Lencioni R, Koike K, Zucman-Rossi J and Finn RS: Hepatocellular carcinoma. Nat Rev Dis Primers 7: 6, 2021.
5. Marrero JA, Kulik LM, Sirlin CB, Zhu AX, Finn RS, Abecassis MM, Roberts LR and Heimbach JK: Diagnosis, staging, and management of hepatocellular carcinoma: 2018 Practice guidance by the american association for the study of liver diseases. Hepatology 68: 723-750, 2018.
6. Kluger MD, Salceda JA, Laurent A, Tayar C, Duvoux C, Decaens T, Luciani A, Van Nhieu JT, Azoulay D and Cherqui D: Liver resection for hepatocellular carcinoma in 313 western patients: Tumor biology and underlying liver rather than tumor size drive prognosis. J Hepatol 62: 1131-1140, 2015.
7. Zhao L, Wu X, Li T, Luo J and Dong D: ctcRbase: The gene expression database of circulating tumor cells and microemboli. Database (Oxford) 2020: baaa020, 2020.
8. Alix-Panabières C and Pantel K: Circulating tumor cells: Liquid biopsy of cancer. Clin Chem 59: 110-118, 2013.
9. Allard WJ, Matera J, Miller MC, Repollet M, Connelly MC, Rao C, Tibbe AG, Uhr JW and Terstappen LW: Tumor cells circulate in the peripheral blood of all major carcinomas but not in healthy subjects or patients with nonmalignant diseases. Clin Cancer Res 10: 6897-6904, 2004.
10. Plaks V, Koopman CD and Werb Z: Cancer. Circulating tumor cells. Science 341: 1186-1188, 2013.
11. Szczerba BM, Castro-Giner F, Vetter M, Krol I, Gkountela S, Landin J, Scheidmann MC, Donato C, Scherrer R, Singer J, *et al*: Neutrophils escort circulating tumour cells to enable cell cycle progression. Nature 566: 553-557, 2019.
12. Aceto N, Bardia A, Miyamoto DT, Donaldson MC, Wittner BS, Spencer JA, Yu M, Pely A, Engstrom A, Zhu H, *et al*: Circulating tumor cell clusters are oligoclonal precursors of breast cancer metastasis. Cell 158: 1110-1122, 2014.
13. Lo HC, Xu Z, Kim IS, Pingel B, Aguirre S, Kodali S, Liu J, Zhang W, Muscarella AM, Hein SM, *et al*: Resistance to natural killer cell immunosurveillance confers a selective advantage to polyclonal metastasis. Nat Cancer 1: 709-722, 2020.
14. Pereira-Veiga T, Schneegans S, Pantel K and Wikman H: Circulating tumor cell-blood cell crosstalk: Biology and clinical relevance. Cell Rep 40: 111298, 2022.
15. Cristofanilli M, Budd GT, Ellis MJ, Stopeck A, Matera J, Miller MC, Reuben JM, Doyle GV, Allard WJ, Terstappen LW and Hayes DF: Circulating tumor cells, disease progression, and survival in metastatic breast cancer. N Engl J Med 351: 781-791, 2004.
16. Hou JM, Krebs MG, Lancashire L, Sloane R, Backen A, Swain RK, Priest LJ, Greystoke A, Zhou C, Morris K, *et al*: Clinical significance and molecular characteristics of circulating tumor cells and circulating tumor microemboli in patients with small-cell lung cancer. J Clin Oncol 30: 525-532, 2012.
17. Ye Q, Ling S, Zheng S and Xu X: Liquid biopsy in hepatocellular carcinoma: Circulating tumor cells and circulating tumor DNA. Mol Cancer 18: 114, 2019.
18. De Rubis G, Rajeev Krishnan S and Bebawy M: Liquid biopsies in cancer diagnosis, monitoring, and prognosis. Trends Pharmacol Sci 40: 172-186, 2019.
19. Yu JJ, Xiao W, Dong SL, Liang HF, Zhang ZW, Zhang BX, Huang ZY, Chen YF, Zhang WG, Luo HP, *et al*: Effect of surgical liver resection on circulating tumor cells in patients with hepatocellular carcinoma. BMC Cancer 18: 835, 2018.
20. Kelley RK, Magbanua MJ, Butler TM, Collisson EA, Hwang J, Sidiropoulos N, Evason K, McWhirter RM, Hameed B, Wayne EM, *et al*: Circulating tumor cells in hepatocellular carcinoma: A pilot study of detection, enumeration, and next-generation sequencing in cases and controls. BMC Cancer 15: 206, 2015.
21. Sun YF, Xu Y, Yang XR, Guo W, Zhang X, Qiu SJ, Shi RY, Hu B, Zhou J and Fan J: Circulating stem cell-like epithelial cell adhesion molecule-positive tumor cells indicate poor prognosis of hepatocellular carcinoma after curative resection. Hepatology 57: 1458-1468, 2013.
22. Wang Y and Navin NE: Advances and applications of single-cell sequencing technologies. Mol Cell 58: 598-609, 2015.
23. Abouleila Y, Onidani K, Ali A, Shoji H, Kawai T, Lim CT, Kumar V, Okaya S, Kato K, Hiyama E, *et al*: Live single cell mass spectrometry reveals cancer-specific metabolic profiles of circulating tumor cells. Cancer Sci 110: 697-706, 2019.
24. Bhan I, Mosesso K, Goyal L, Philipp J, Kalinich M, Franses JW, Choz M, Oklu R, Toner M, Maheswaran S, *et al*: Detection and analysis of circulating epithelial cells in liquid biopsies from patients with liver disease. Gastroenterology 155: 2016-2018.e11, 2018.
25. Mariathasan S, Turley SJ, Nickles D, Castiglioni A, Yuen K, Wang Y, Kadel EE III, Koeppen H, Astarita JL, Cubas R, *et al*: TGFβ attenuates tumour response to PD-L1 blockade by contributing to exclusion of T cells. Nature 554: 544-548, 2018.
26. Yu G, Wang LG, Han Y and He QY: clusterProfiler: An R package for comparing biological themes among gene clusters. OMICS 16: 284-287, 2012.
27. Subramanian A, Tamayo P, Mootha VK, Mukherjee S, Ebert BL, Gillette MA, Paulovich A, Pomeroy SL, Golub TR, Lander ES and Mesirov JP: Gene set enrichment analysis: A knowledge-based approach for interpreting genome-wide expression profiles. Proc Natl Acad Sci USA 102: 15545-15550, 2005.
28. Bader GD and Hogue CW: An automated method for finding molecular complexes in large protein interaction networks. BMC Bioinformatics 4: 2, 2003.
29. Chin CH, Chen SH, Wu HH, Ho CW, Ko MT and Lin CY: cytoHubba: Identifying hub objects and sub-networks from complex interactome. BMC Syst Biol 8 (Suppl 4): S11, 2014.
30. Hänzelmann S, Castelo R and Guinney J: GSVA: Gene set variation analysis for microarray and RNA-seq data. BMC Bioinformatics 14: 7, 2013.
31. Tibshirani R: The lasso method for variable selection in the Cox model. Stat Med 16: 385-395, 1997.
32. Lossos IS, Czerwinski DK, Alizadeh AA, Wechser MA, Tibshirani R, Botstein D and Levy R: Prediction of survival in diffuse large-B-cell lymphoma based on the expression of six genes. N Engl J Med 350: 1828-1837, 2004.
33. Gaujoux R and Seoighe C: A flexible R package for nonnegative matrix factorization. BMC Bioinformatics 11: 367, 2010.
34. Iasonos A, Schrag D, Raj GV and Panageas KS: How to build and interpret a nomogram for cancer prognosis. J Clin Oncol 26: 1364-1370, 2008.
35. Newman AM, Liu CL, Green MR, Gentles AJ, Feng W, Xu Y, Hoang CD, Diehn M and Alizadeh AA: Robust enumeration of cell subsets from tissue expression profiles. Nat Methods 12: 453-457, 2015.
36. Li T, Fan J, Wang B, Traugh N, Chen Q, Liu JS, Li B and Liu XS: TIMER: A web server for comprehensive analysis of tumor-infiltrating immune cells. Cancer Res 77: e108-e110, 2017.
37. Finotello F, Mayer C, Plattner C, Laschober G, Rieder D, Hackl H, Krogsdam A, Loncova Z, Posch W, Wilflingseder D, *et al*: Molecular and pharmacological modulators of the tumor immune contexture revealed by deconvolution of RNA-seq data. Genome Med 11: 34, 2019.
38. Becht E, Giraldo NA, Lacroix L, Buttard B, Elarouci N, Petitprez F, Selves J, Laurent-Puig P, Sautès-Fridman C, Fridman WH and de Reyniès A: Estimating the population abundance of tissue-infiltrating immune and stromal cell populations using gene expression. Genome Biol 17: 218, 2016.
39. Aran D, Hu Z and Butte AJ: xCell: Digitally portraying the tissue cellular heterogeneity landscape. Genome Biol 18: 220, 2017.
40. Sturm G, Finotello F, Petitprez F, Zhang JD, Baumbach J, Fridman WH, List M and Aneichyk T: Comprehensive evaluation of transcriptome-based cell-type quantification methods for immuno-oncology. Bioinformatics 35: i436-i445, 2019.
41. Racle J and Gfeller D: EPIC: A tool to estimate the proportions of different cell types from bulk gene expression data. Methods Mol Biol 2120: 233-248, 2020.

42. Zeng D, Ye Z, Shen R, Yu G, Wu J, Xiong Y, Zhou R, Qiu W, Huang N, Sun L, *et al*: IOBR: Multi-omics immuno-oncology biological research to decode tumor microenvironment and signatures. Front Immunol 12: 687975, 2021.
43. Malta TM, Sokolov A, Gentles AJ, Burzykowski T, Poisson L, Weinstein JN, Kamińska B, Huelsken J, Omberg L, Gevaert O, *et al*: Machine learning identifies stemness features associated with oncogenic dedifferentiation. Cell 173: 338-354. e15, 2018.
44. Yang W, Soares J, Greninger P, Edelman EJ, Lightfoot H, Forbes S, Bindal N, Beare D, Smith JA, Thompson IR, *et al*: Genomics of drug sensitivity in cancer (GDSC): A resource for therapeutic biomarker discovery in cancer cells. Nucleic Acids Res 41: D955-D961, 2013.
45. Ozga AJ, Chow MT and Luster AD: Chemokines and the immune response to cancer. Immunity 54: 859-874, 2021.
46. Vilgelm AE and Richmond A: Chemokines modulate immune surveillance in tumorigenesis, metastasis, and response to immunotherapy. Front Immunol 10: 333, 2019.
47. Ru B, Wong CN, Tong Y, Zhong JY, Zhong SSW, Wu WC, Chu KC, Wong CY, Lau CY, Chen I, *et al*: TISIDB: An integrated repository portal for tumor-immune system interactions. Bioinformatics 35: 4200-4202, 2019.
48. Du Y, Ma Y, Zhu Q, Liu T, Jiao Y, Yuan P and Wang X: An m6A-related prognostic biomarker associated with the hepatocellular carcinoma immune microenvironment. Front Pharmacol 12: 707930, 2021.
49. Fu XW and Song CQ: Identification and validation of pyroptosis-related gene signature to predict prognosis and reveal immune infiltration in hepatocellular carcinoma. Front Cell Dev Biol 9: 748039, 2021.
50. Guo DZ, Huang A, Wang YP, Cao Y, Fan J, Yang XR and Zhou J: Development of an eight-gene prognostic model for overall survival prediction in patients with hepatocellular carcinoma. J Clin Transl Hepatol 9: 898-908, 2021.
51. Lei D, Chen Y, Zhou Y, Hu G and Luo F: A starvation-Based 9-mRNA signature correlates with prognosis in patients with hepatocellular carcinoma. Front Oncol 11: 716757, 2021.
52. Tian D, Yu Y, Zhang L, Sun J and Jiang W: A five-gene-based prognostic signature for hepatocellular carcinoma. Front Med (Lausanne) 8: 681388, 2021.
53. Zheng S, Xie X, Guo X, Wu Y, Chen G, Chen X, Wang M, Xue T and Zhang B: Identification of a pyroptosis-related gene signature for predicting overall survival and response to immunotherapy in hepatocellular carcinoma. Front Genet 12: 789296, 2021.
54. Qi LN, Xiang BD, Wu FX, Ye JZ, Zhong JH, Wang YY, Chen YY, Chen ZS, Ma L, Chen J, *et al*: Circulating tumor cells undergoing EMT provide a metric for diagnosis and prognosis of patients with hepatocellular carcinoma. Cancer Res 78: 4731-4744, 2018.
55. Schilling D, Todenhöfer T, Hennenlotter J, Schwentner C, Fehm T and Stenzl A: Isolated, disseminated and circulating tumour cells in prostate cancer. Nat Rev Urol 9: 448-463, 2012.
56. Zhou H, Zhu L, Song J, Wang G, Li P, Li W, Luo P, Sun X, Wu J, Liu Y, *et al*: Liquid biopsy at the frontier of detection, prognosis and progression monitoring in colorectal cancer. Mol Cancer 21: 86, 2022.
57. Diamantopoulou Z, Castro-Giner F, Schwab FD, Foerster C, Saini M, Budinjas S, Strittmatter K, Krol I, Seifert B, Heinzelmann-Schwarz V, *et al*: The metastatic spread of breast cancer accelerates during sleep. Nature 607: 156-162, 2022.
58. Magri V, Marino L, Nicolazzo C, Gradilone A, De Renzi G, De Meo M, Gandini O, Sabatini A, Santini D, Cortesi E and Gazzaniga P: Prognostic role of circulating tumor cell trajectories in metastatic colorectal cancer. Cells 12: 1172, 2023.
59. Xie J, Wang B, Luo W, Li C and Jia X: Upregulation of KIF18B facilitates malignant phenotype of esophageal squamous cell carcinoma by activating CDCA8/mTORC1 pathway. J Clin Lab Anal 36: e24633, 2022.
60. Xiang C, Sun WH, Ke Y, Yu X and Wang Y: CDCA8 contributes to the development and progression of thyroid cancer through regulating CDK1. J Cancer 13: 2322-2335, 2022.
61. Ci C, Tang B, Lyu D, Liu W, Qiang D, Ji X, Qiu X, Chen L and Ding W: Overexpression of CDCA8 promotes the malignant progression of cutaneous melanoma and leads to poor prognosis. Int J Mol Med 43: 404-412, 2019.
62. Jeon T, Ko MJ, Seo YR, Jung SJ, Seo D, Park SY, Park KU, Kim KS, Kim M, Seo JH, *et al*: Silencing CDCA8 suppresses hepatocellular carcinoma growth and stemness via restoration of ATF3 tumor suppressor and inactivation of AKT/β-catenin signaling. Cancers (Basel) 13: 1055, 2021.
63. Wang Y, Martin TA and Jiang WG: HAVcR-1 expression in human colorectal cancer and its effects on colorectal cancer cells in vitro. Anticancer Res 33: 207-214, 2013.
64. Zheng X, Xu K, Chen L, Zhou Y and Jiang J: Prognostic value of TIM-1 expression in human non-small-cell lung cancer. J Transl Med 17: 178, 2019.
65. Cuadros T, Trilla E, Sarró E, Vilà MR, Vilardell J, de Torres I, Salcedo M, López-Hellin J, Sánchez A, Ramón y Cajal S, *et al*: HAVCR/KIM-1 activates the IL-6/STAT-3 pathway in clear cell renal cell carcinoma and determines tumor progression and patient outcome. Cancer Res 74: 1416-1428, 2014.
66. Ye L, Zhang Q, Cheng Y, Chen X, Wang G, Shi M, Zhang T, Cao Y, Pan H, Zhang L, *et al*: Tumor-derived exosomal HMGB1 fosters hepatocellular carcinoma immune evasion by promoting TIM-1^{+} regulatory B cell expansion. J Immunother Cancer 6: 145, 2018.
67. Gu MM, Gao D, Yao PA, Yu L, Yang XD, Xing CG, Zhou J, Shang ZF and Li M: p53-inducible gene 3 promotes cell migration and invasion by activating the FAK/Src pathway in lung adenocarcinoma. Cancer Sci 109: 3783-3793, 2018.
68. Li M, Li S, Liu B, Gu MM, Zou S, Xiao BB, Yu L, Ding WQ, Zhou PK, Zhou J and Shang ZF: PIG3 promotes NSCLC cell mitotic progression and is associated with poor prognosis of NSCLC patients. J Exp Clin Cancer Res 36: 39, 2017.
69. Qin XY, Suzuki H, Honda M, Okada H, Kaneko S, Inoue I, Ebisui E, Hashimoto K, Carninci P, Kanki K, *et al*: Prevention of hepatocellular carcinoma by targeting MYCN-positive liver cancer stem cells with acyclic retinoid. Proc Natl Acad Sci USA 115: 4969-4974, 2018.
70. Qin XY, Su T, Yu W and Kojima S: Lipid desaturation-associated endoplasmic reticulum stress regulates MYCN gene expression in hepatocellular carcinoma cells. Cell Death Dis 11: 66, 2020.
71. Lee D, Xu IMJ, Chiu DKC, Leibold J, Tse APW, Bao MHR, Yuen VWH, Chan CYK, Lai RKH, Chin DWC, *et al*: Induction of oxidative stress through inhibition of thioredoxin reductase 1 is an effective therapeutic approach for hepatocellular carcinoma. Hepatology 69: 1768-1786, 2019.
72. Muñoz-Gámez JA, López Viota J, Barrientos A, Carazo Á, Sanjuán-Nuñez L, Quiles-Perez R, Muñoz-de-Rueda P, Delgado Á, Ruiz-Extremera Á and Salmerón J: Synergistic cytotoxicity of the poly (ADP-ribose) polymerase inhibitor ABT-888 and temozolomide in dual-drug targeted magnetic nanoparticles. Liver Int 35: 1430-1441, 2015.
73. Wang S, Liu J, Wu H, Jiang A, Zhao K, Yan K, Wu W, Han H, Zhang Y and Yang W: All-trans retinoic acid (ATRA) inhibits insufficient radiofrequency ablation (IRFA)-induced enrichment of tumor-initiating cells in hepatocellular carcinoma. Chin J Cancer Res 33: 694-707, 2021.
74. Sun J, Liu C, Shi J, Wang N, Jiang D, Mao F, Gu J, Zhou L, Shen L, Lau WY and Cheng S: A novel chemotherapy strategy for advanced hepatocellular carcinoma: A multicenter retrospective study. Chin Med J (Engl) 135: 2338-2343, 2022.
75. Augello G, Emma MR, Cusimano A, Azzolina A, Mongiovì S, Puleio R, Cassata G, Gulino A, Belmonte B, Gramignoli R, *et al*: Targeting HSP90 with the small molecule inhibitor AUY922 (luminespib) as a treatment strategy against hepatocellular carcinoma. Int J Cancer 144: 2613-2624, 2019.
76. Jiang P, Gu S, Pan D, Fu J, Sahu A, Hu X, Li Z, Traugh N, Bu X, Li B, *et al*: Signatures of T cell dysfunction and exclusion predict cancer immunotherapy response. Nat Med 24: 1550-1558, 2018.
77. Lee JO, Lee KW, Oh DY, Kim JH, Im SA, Kim TY and Bang YJ: Combination chemotherapy with capecitabine and cisplatin for patients with metastatic hepatocellular carcinoma. Ann Oncol 20: 1402-1407, 2009.
78. Li L, Zhang Y, Zhou Y, Hu H, Hu Y, Georgiades C, Mao HQ and Selaru FM: Quaternary nanoparticles enable sustained release of bortezomib for hepatocellular carcinoma. Hepatology 76: 1660-1672, 2022.
79. Zhu AX, Blaszkowsky LS, Ryan DP, Clark JW, Muzikansky A, Horgan K, Sheehan S, Hale KE, Enzinger PC, Bhargava P and Stuart K: Phase II study of gemcitabine and oxaliplatin in combination with bevacizumab in patients with advanced hepatocellular carcinoma. J Clin Oncol 24: 1898-1903, 2006.